Characterization and Analysis of Long Term Field Aged Photovoltaic Modules and Encapsulant Materials

by

Matthew Chicca

A Thesis Presented in Partial Fulfillment
of the Requirements for the Degree
Master of Science

Approved November 2015 by the
Graduate Supervisory Committee:

Govindasamy Tamizhmani, Chair
Devarajan Srinivasan
Bradley Rogers

ARIZONA STATE UNIVERSITY

December 2015

ABSTRACT

Photovoltaic (PV) module degradation is a well-known issue, however understanding the mechanistic pathways in which modules degrade is still a major task for the PV industry. In order to study the mechanisms responsible for PV module degradation, the effects of these degradation mechanisms must be quantitatively measured to determine the severity of each degradation mode. In this thesis multiple modules from three climate zones (Arizona, California and Colorado) were investigated for a single module glass/polymer construction (Siemens M55) to determine the degree to which they had degraded, and the main factors that contributed to that degradation. To explain the loss in power, various nondestructive and destructive techniques were used to indicate possible causes of loss in performance. This is a two-part thesis. Part 1 presents non-destructive test results and analysis and Part 2 presents destructive test results and analysis.

To,
My parents, Edward and Nancy Chicca, and other friends and family members for their constant support and love

ACKNOWLEDGMENTS

I would like first and foremost to thank professor Dr. Govindasamy Tamizhmani for accepting me into his lab providing me this amazing opportunity, and for his constant support throughout my thesis work. I consider myself very fortunate to have been given all the opportunities that working with him have afforded me. I would like to thank my fellow lab students for their support, and I would specifically like to thank Sai Tatapudi, our technical lab manager, and Christopher Raupp, a fellow lab student, for their unwavering guidance and support. I would also like to thank Dr. Jordan Dirk and Dr. John Wolgemuth, from the National Renewable Energy Laboratories, NREL, for the opportunity to work with them on their projects.

TABLE OF CONTENTS

Page

Page

LIST OF TABLES

Table Page

LIST OF FIGURES

Figure Page

PART 1: NON-DESTRUCTIVE ANALYSIS OF FIELD AGED MODULES

CHAPTER 1

INTRODUCTION

This is a two-part thesis. The non-destructive test results and analysis are presented in Part 1 and destructive test results and analysis are presented in Part 2.

1.1.1 Background

In the last decade photovoltaic (PV) industry has taken on a major role in power generation throughout America and the world. Photovoltaic modules provide many advantages that today grid is not able to mainly in developing countries, by providing on-site localized power generation where gridlines cannot or have not reached yet. However, the materials of all PV modules degrade over time and the power generation degrades with them. By understanding the way in which modules degrade new advances can be made in increasing the longevity of module lifetime.

1.1.2 Scope of Work

Photovoltaic (PV) module degradation in the field is a known issue, however, understanding the modes and mechanisms in which modules degrade is still a major undertaking for researchers. To understand the degradation modes and mechanisms, both nondestructive and destructive characterization techniques need to be employed. This part of the report presents the use of nondestructive techniques and corresponding results. In this report several eighteen years old modules exposed in a hot-dry climate (Tempe, Arizona), 28 years old modules in a temperate climate (Sacramento, California) and 20

years old modules in a temperate/cold climate (Golden, Colorado) were investigated to identify the degradation modes and to determine the degree to which they had degraded the performance of the module. The nondestructive techniques utilized in this work are: current-voltage measurements (I-V), visual inspection (VI), diode failure (DF), infrared (IR) imaging, electroluminescence (EL) imaging, dark current-voltage (D-I-V) nondestructive cell-module quantum efficiency (C-M-QE), and module level reflectance spectroscopy (M-RS).

The power output of PV modules is affected by the deterioration of one or more of the following three I-V parameters (response variables): short circuit current; open circuit voltage; fill factor (due to series resistance increase and/or shunt resistance decrease). These response parameters are typically affected by several degradation modes (predictor variables) including discoloration of encapsulant, cell interconnect ribbon cracks, solder bond fatigue, and more. These two variables would be sufficient to generate correlation plots correlating degradation modes responsible for specific I-V parameter degradation [1-3]. This paper provides non-destructive techniques to identify all the response variables and most of the predictor variables. Additional destructive techniques may be needed to identify some of the predictor variables which are not identified by the non-destructive techniques. It is to be noted that these techniques will, most likely, not be sufficient to determine the degradation mechanisms responsible for the degradation modes, and hence a physics- or chemistry-based lifetime prediction model cannot be developed based on the information provided in this report alone.

CHAPTER 2

METHODOLOGY

The nondestructive techniques utilized in this work are: current-voltage measurement (I-V), visual inspection (VI), diode failure (DF), infrared (IR) imaging, electroluminescence (EL) imaging, UV fluorescence (UVF), dark I-V (D-I-V), module level quantum efficiency (M-QE), and module level reflectance spectroscopy (M-RS). Since the purpose of most of these techniques is already known, it is explained only very briefly in this section.

1.2.1 Current-Voltage (I-V) Measurements

The I-V data was collected using a Daystar I-V curve tracer under natural sunlight. Two reference cells were used during data collection to ensure accurate readings, one crystalline silicon and one poly silicon reference cell. A thermocouple was attached to the center of each module to monitor the temperature of the module and an additional thermocouple was used to measure the ambient temperature. An indoor AAA flash tester was used to validate the outdoor data obtained under natural sunlight. Based on the I-V data and the number of years of field exposure, the degradation rates of individual modules were determined, along with the temperature coefficients. The light I-V based series and shunt resistances were also calculated. (Picture of curve tracer set up)

1.2.2 Visual Inspection (VI)

The modules were inspected using the visual inspection checklist developed by National Renewable Energy Laboratory (NREL). The conditions of the modules were visually and photographically examined to determine the visual defects or failures. Findings from the visual inspection were then used to generate: a visual defect Pareto chart to identify all the visual defects in decreasing order.

1.2.3 Diode Failure (DF)

Diode functionality (open circuit or short circuit) was verified by use of a diode checker. If diodes fail in the short-circuited mode it will lead to the power loss and if they fail in the open-circuited mode modules could lead to fire hazard or electrical safety issue. To check the diodes a line checker was used. The current generator was plugged into the module and a small amount of current was sent through the module. If the module was not shaded and no beep was heard then that particular string was being bypassed resulting from another issue. If the module was being shaded and a beep was heard than the diode was not working properly because that string should have been bypassed.

1.2.4 Infrared Imaging (IR)

The modules were placed outside and put under short circuit or loaded conditions. IR imaging study was conducted to assess whether or not the modules had any hotspot

cells (hotspot cells within the module are defined as the cells that are operating at or above 20°C higher than the average temperature of all the cells within the module). These hotspots could eventually lead to accelerated power degradation or safety failures including backsheet delamination or burning and solder bond issues. Modules were left outside under short circuit conditions for approximately 10 minutes before an image was taken using Fluke Tir2 Ft Thermal Imager camera, the images were processed and altered using SmartView software to more clearly highlight the areas of interest.

1.2.5 Electroluminescence Imaging (EL)

Semiconductors in photovoltaic modules usually convert light into electrical energy, however due to their unique properties if the process is applied in the reverse order semiconductors will produce light as excess electrons are excited up to the conduction band. This phenomenon is known as electroluminescence and it serves as a useful tool for module characterization. In order to identify areas of cell in a module where current is not reaching easily or at all an external power supply is connected to a module and a voltage and current up to 1.33*the measured Isc value is applied to the module in a dark room under forward bias conditions. A sensovation HR-830 pro camera was used on a 30 second exposure time to obtain the EL images. The modules being investigated had junction boxes on opposite ends so special attention was given to ensure that the positive side junction box was always placed on the left side of the image. Once the high resolution images were captured details such as cell cracks, cell shunting and cell metallization adhesion issues were able to be seen.

1.2.6 UV Fluorescence Imaging (UVF)

In general fluorescence occurs when an orbital electron of a molecule relaxes down to a ground state from an excited state. In Aged EVA fluorescence occurs due to chromophores that have developed within EVA as a result of its degradation. This technique is useful for identifying browned EVA, possible cell cracks, and cracked backsheet. To investigate the modules using UV fluorescence a UV lamp was used to illuminate each module and pictures were taken to show areas where EVA had browned.

1.2.7 Dark I-V (D-I-V)

The dark I-V measurements were carried out indoor under controlled temperature conditions to obtain dark series and shunt resistances measurements. Dark I-V measurements serve as a valuable analysis tool for investigating diode properties of modules.

1.2.8 Module Level Quantum Efficiency (C-M-QE)

A non-destructive cell-module QE (C-M-QE) was performed using PV measurement's Solar Panel Quantum Efficiency Measurement System, model QEX12M to obtain QE losses in the shunted regions (if any based on EL imaging), heavily browned encapsulant cell center regions and clear cell edge regions. I n addition to the edge of cell and center of cell comparison within a module, center of cell measuremnets were compared between control modules and their respective aged modules, and between aged modules of the three environments. These measurements were performed at various

spots of individual cells without cutting the backsheet of the module. A detailed description of this technique is presented elsewhere [4].

1.2.9 Module Level Reflectance Spectroscopy (M-RS)

To measure the reflectance of both control and field aged modules, a fieldspec 4 wide res spectroradiometer was used. The data was processed using viewspec pro software and graphed in excel. By combining the C-M-QE technique with nondestructive module level reflectance spectroscopy technique, the influence wavelength-dependent encapsulant discoloration on short circuit current can be understood. These combined techniques along with other spectroscopic techniques are very powerful methods to determine the degradation mechanism responsible for the encapsulant degradation.

CHAPTER 3

RESULTS AND DISCUSSION

1.3.1 Module Performance Analysis

Visual inspection was done on one fresh module (stored indoor) and nine field aged modules of Siemens M55 Model with nameplate rating of 53 W. A Pareto chart displaying all the visual defects observed on the field exposed modules (18 years) is shown in Figure 1. However, it should be noted that not every visual defect seen on a module will have an effect on the power output of the module. Three defects were seen in every field aged module: EVA browning, frame corrosion and chalking of the backsheet. No delamination or cell damage was observed for these nine field aged modules.

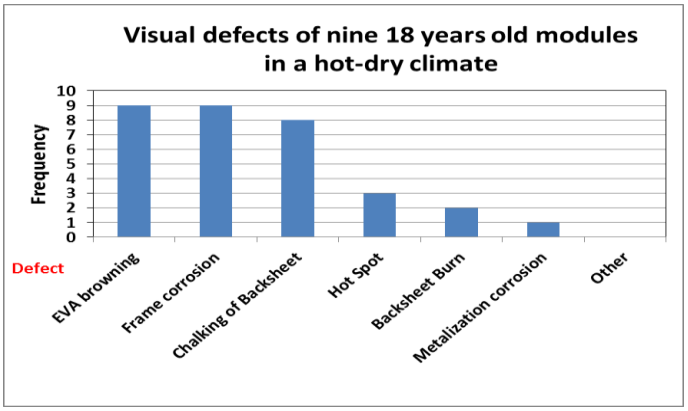

Figure 1: Pareto Chart Showing Visual Defects Observed in Nine, 18 Years Old Modules Using NREL Checklist. "Other" Refers to Anything Else in the Checklist that was or was not Observed.

One of the modules, 514183, had the following defects: backsheet burns, EVA browning, frame corrosion (very minor), hot spots, and backsheet chalking. Not all of these defects

are able to be seen with the naked eye, which is why more detailed analysis is generally needed to fully understand modules' current state of health.

The difference between each field aged module and the control module was calculated for every I-V parameter and is shown in Figure 2-4. The nine modules chosen for the hot dry climate are a subset of 30 modules owned by ASU-PRL and they were all exposed for 18 years in a hot-dry climate of Tempe, Arizona. Three modules were chosen for each category: best, median, and worst based off Pmax alone. These nine modules displayed an average power drop, from the control module, of 21%, FF drop of 21.6%, Isc drop of 2.3%, Voc drop of 1.5%, Imp drop of 6.9%, and a Vmp drop of 16.2%. The SMUD module was exposed in a temperate climate in Sacramento, California for 28 years and it displayed a power drop from the control module of 10.93%, a FF drop of 5.11%, an Isc drop of 6.73%, a Voc dop of 0.65%, an Imp drop of 7.56%, and a Vmp drop of 3.64% . The third set of modules was exposed in a cold dry climate in Denver for 20 years. The Denver modules experienced the least amount of degradation between the three environments at 0.28% per year. This could be attributed to the milder conditions that the modules experienced. The Arizona modules showed an average power drop of 1.16% per year and the SMUD module showed a power drop of 0.39% per year. Arizona modules showed the highest degradation rate per year in every I-V parameter except for I_{sc}. Denver and SMUD showed higher I_{sc} degradation due to the increased browning experience by these modules over their lifetime. Graphs visually displaying the I-V parameters can be found below in figures 2-6.

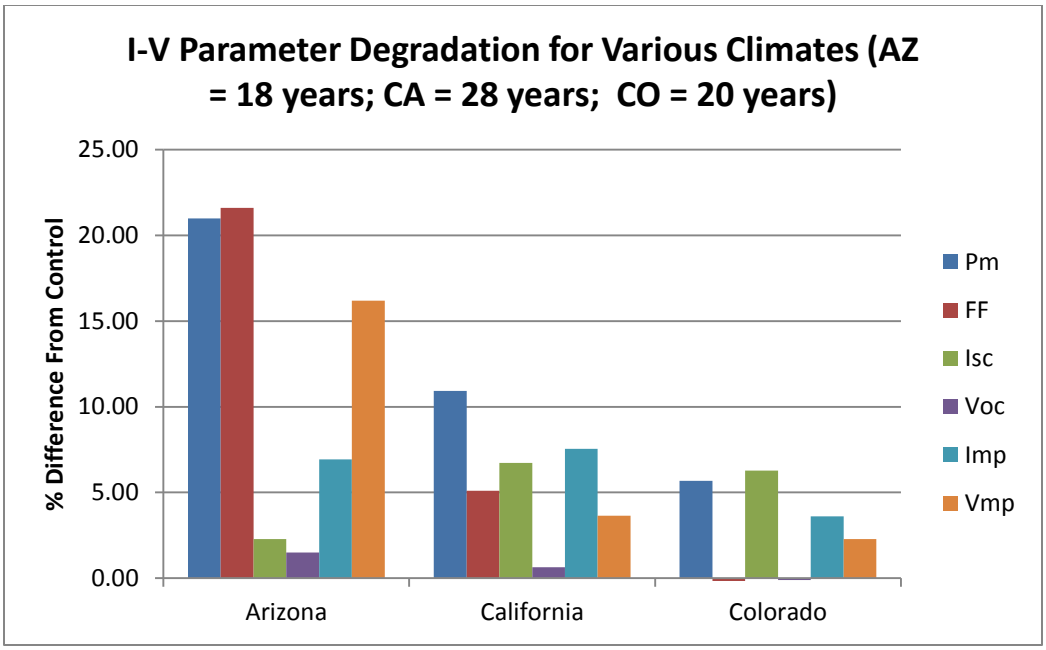

Figure 2: I-V Parameter Degradation for Three Locations.

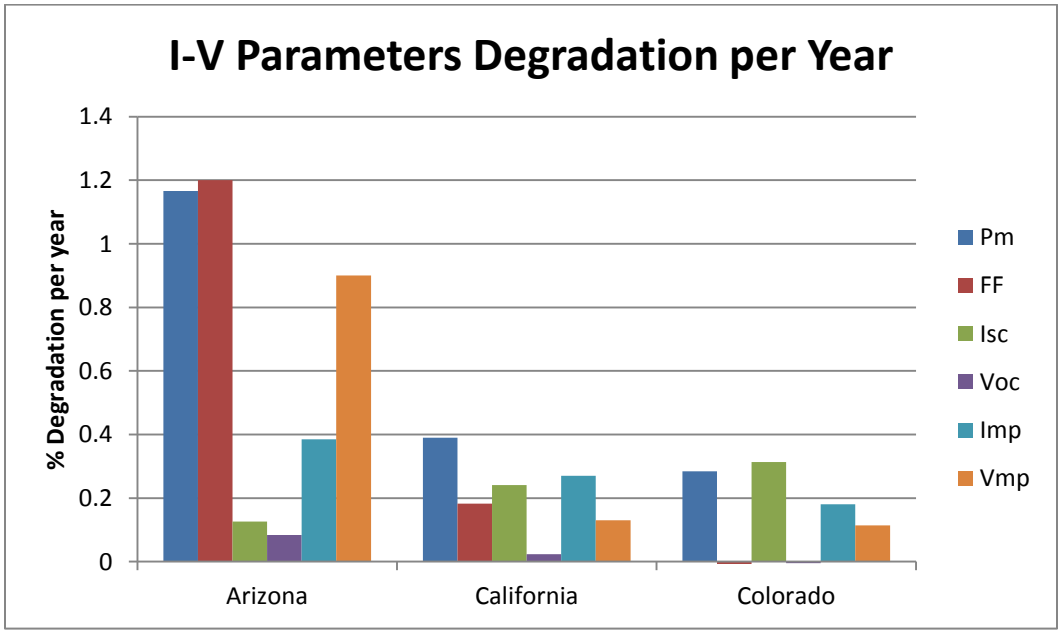

Figure 3: Annual Degradation of Various I-V Parameters for Different Locations

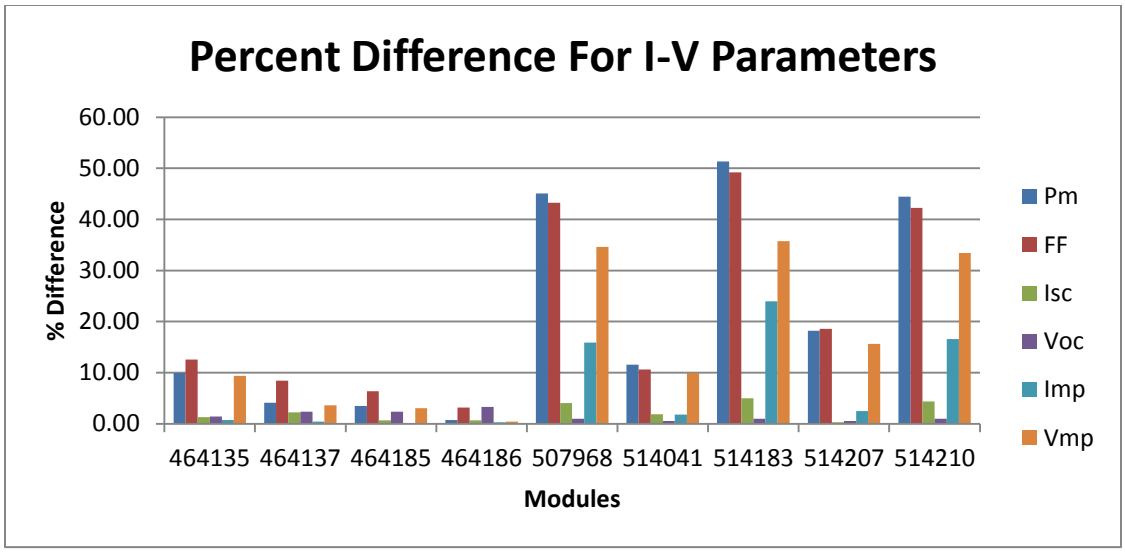

Figure 4: Degradation of I-V parameters for 9 Fielded Modules as Compared to the Control Module Over 18 Years Hot Dry Climate of Arizona

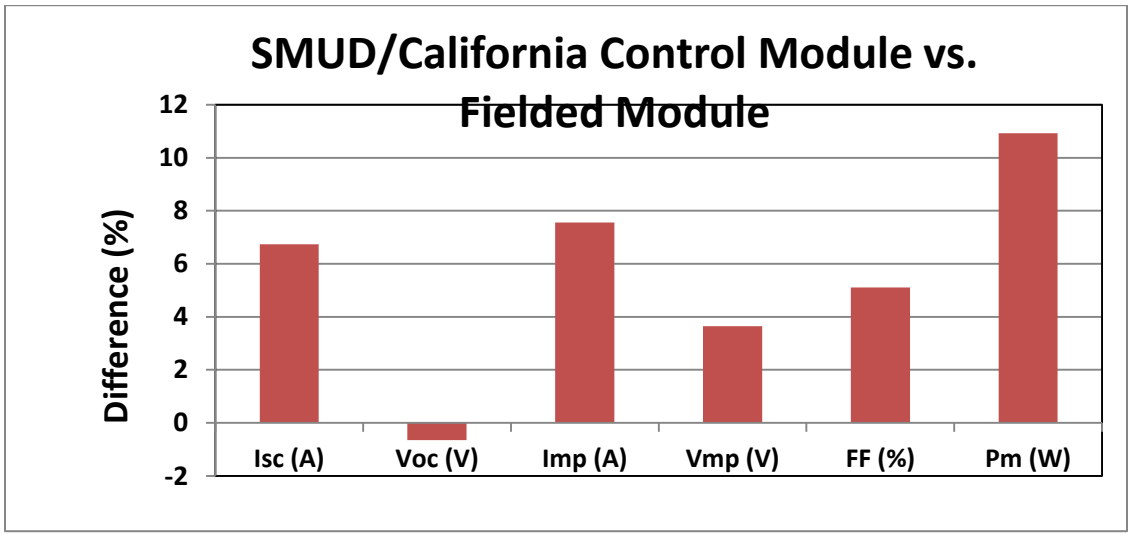

Figure 5: Parameter Loss of Fielded Module as Compared to Control Module

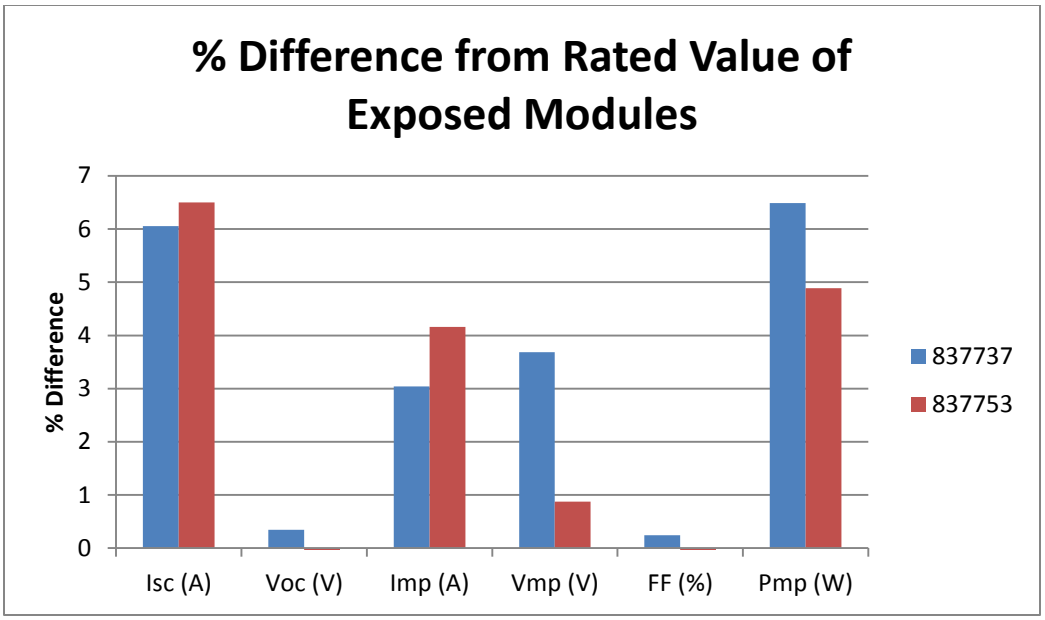

Figure 6: Colorado Modules I-V Parameters

1.3.2 IR and EL Analyses

All Arizona modules were investigated with the aid of Infrared (IR), and electroluminescence (EL) imaging equipment and software. In Figure 7-9, the results of module 514183one of the worst modules, 464186 one of the best modules, and 514207 one of the median modules are shown for the Arizona modules. The multiple hotspots depicted in Figure 7-9 correspond to the bright white spots in the EL image indicating areas where excessive current is being forced to travel through due to the other local solder bonds breaking, or degrading. The dark regions in Figure 7-9 depict both shunted cells, metallization finger detached regions and broken solder bond. Other patterns in this evaluation of all nine modules as shown by IR imaging have indications of hot cells, generally only located over junction boxes.

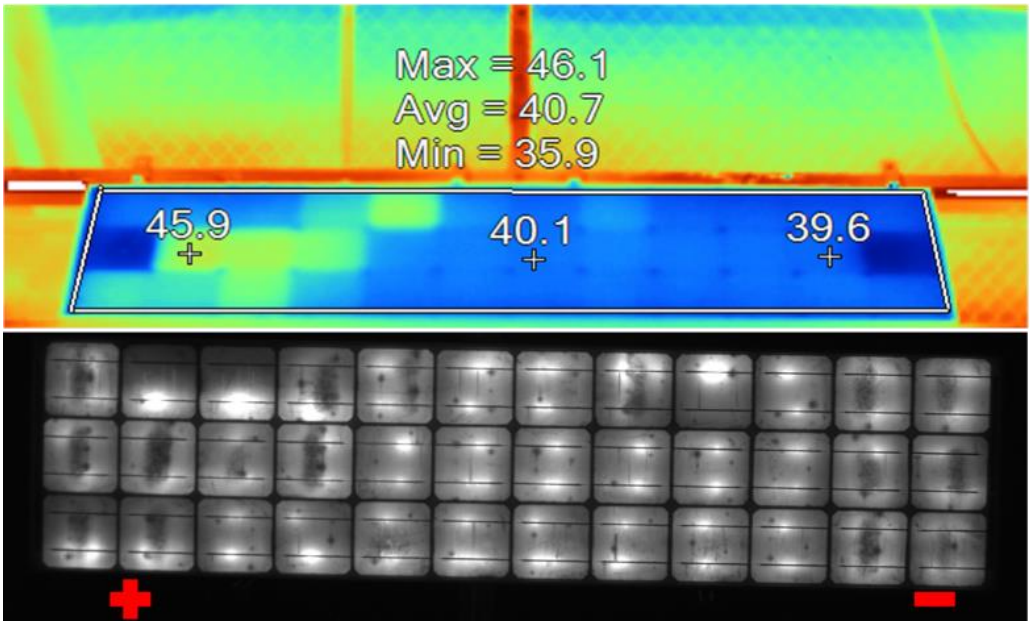

Figure 7: Arizona Module EL (bottom) and IR (top) of Module 464186(best)

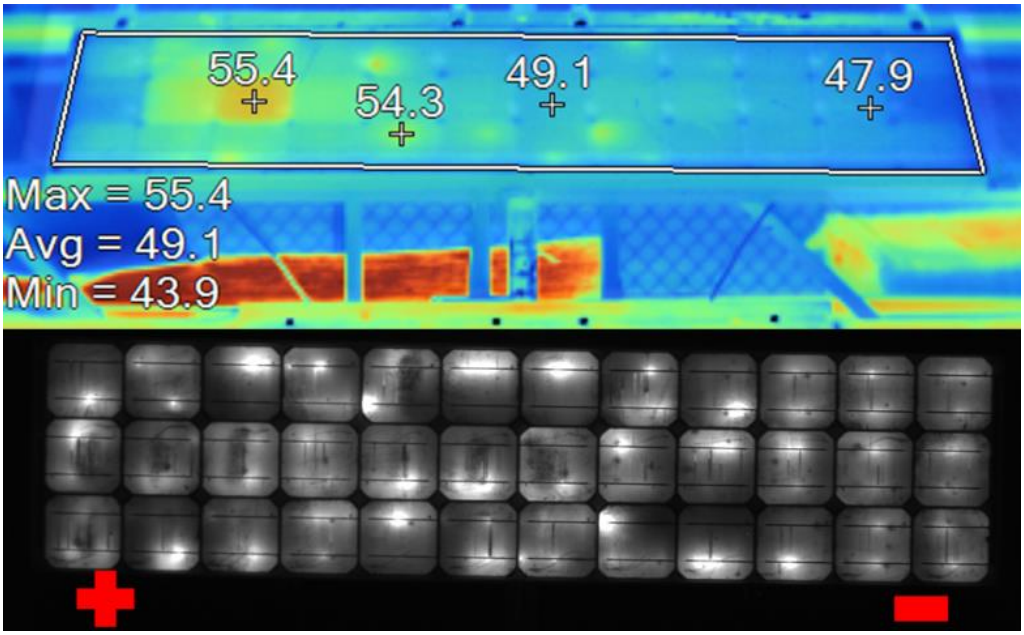

Figure 8: Arizona Module EL (bottom) and IR (top) of Module 514207(median)

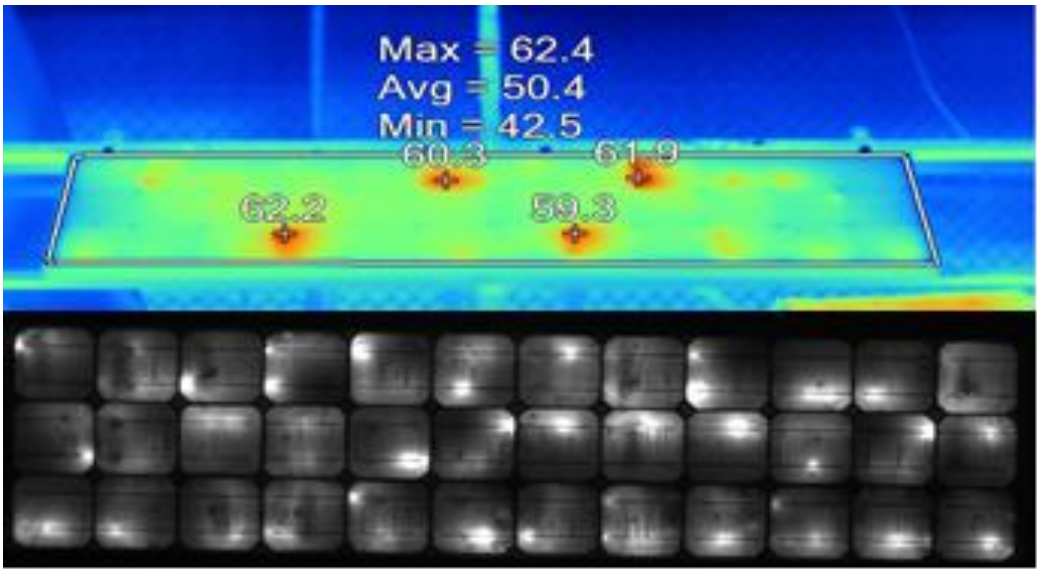

Figure 9: Arizona Module EL (bottom) and IR (top) of Module 514183(worst)

The IR and EL images of the control and field aged SMUD modules is shown in Figure 10 and Figure 11. The positive junction box in these images is on the left side along with the metal plate warning label. These areas combined with the extra heat from the junction box are significantly hotter than the rest of the module due to restricted direct air access to the backsheet. Slightly higher operating temperature of the aged module, in the non-junction box regions, may be attributed to the I^2R heating due to metallization degradation as evidenced in the Rs increase and the temperature coefficient increase.

The IR and EL images of the control and field aged Denver modules is shown in Figure 12 and Figure 13. The EL images clearly indicate that the control module has somehow experienced localized metallization related damages during the storage or it might have been briefly accelerated stress tested leading to metallization damages without causing any browning. These damages may not be severe enough to affect the performance or Isc of the cell as there is no browning issue but they are expected to affect localized QE curves obtained in spots of each cell as discussed later.

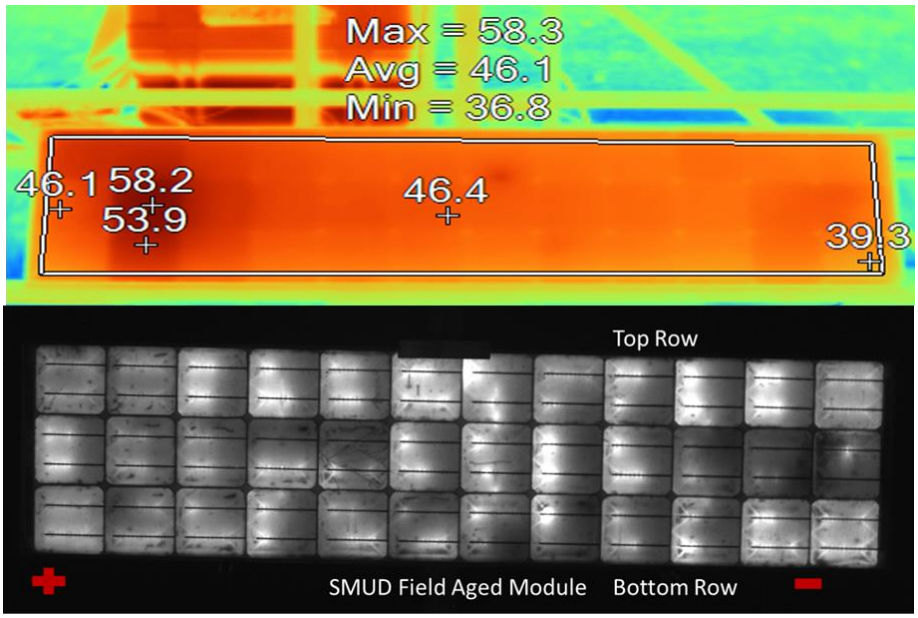

Figure 10: California SMUD aged module IR (Top) and EL(bottom)

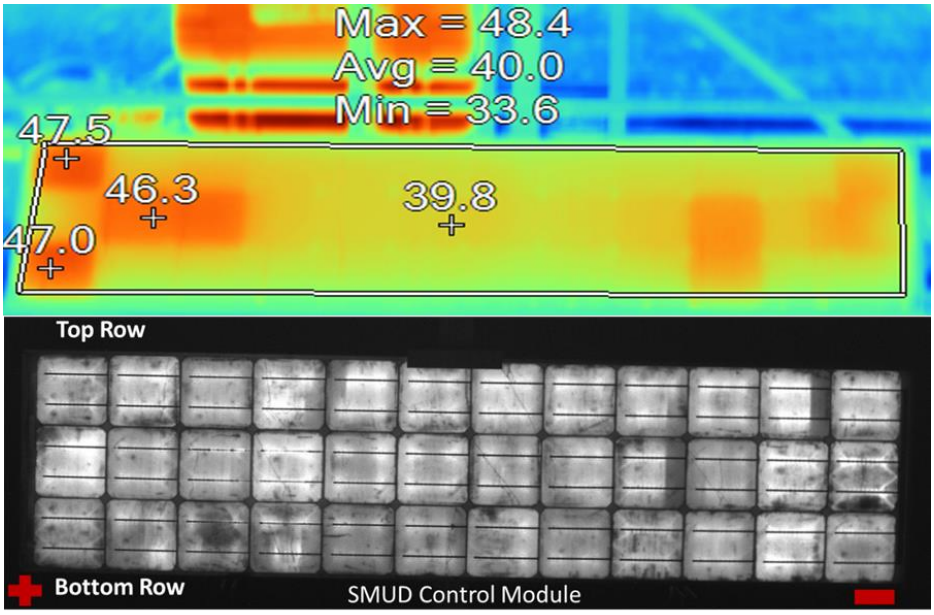

Figure 11: California SMUD Control Module IR (Top) and EL(bottom)

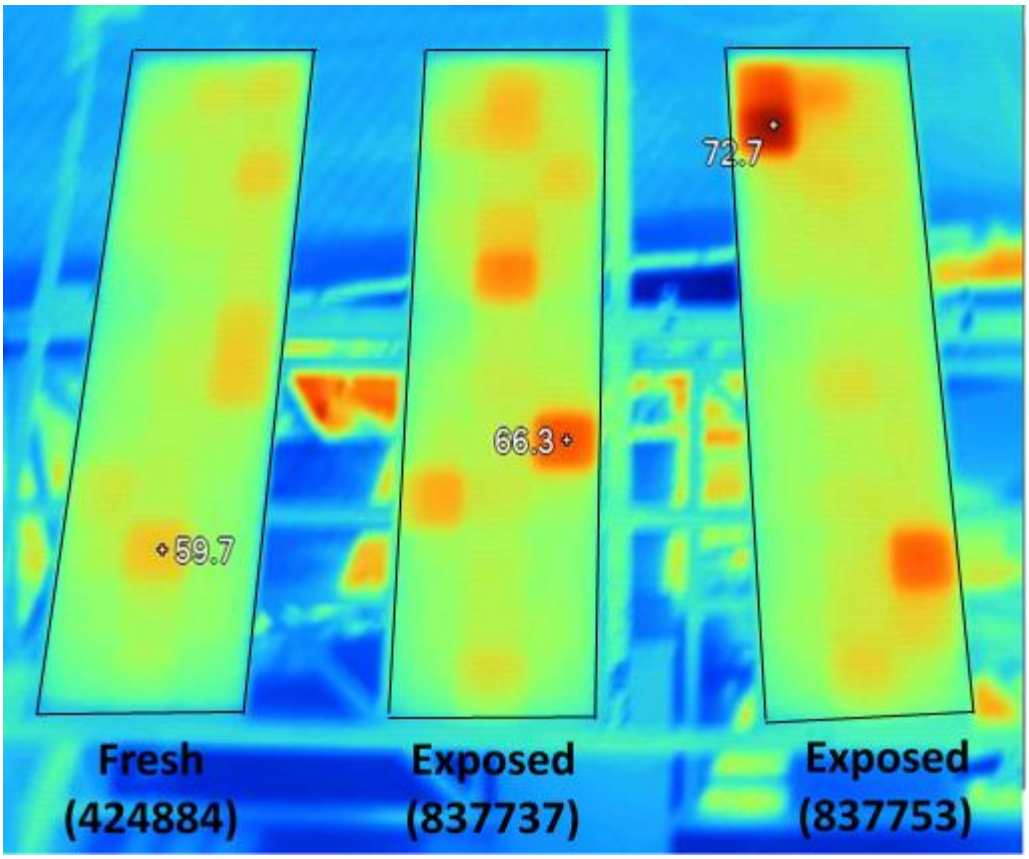

Figure 12: IR of Denver Modules

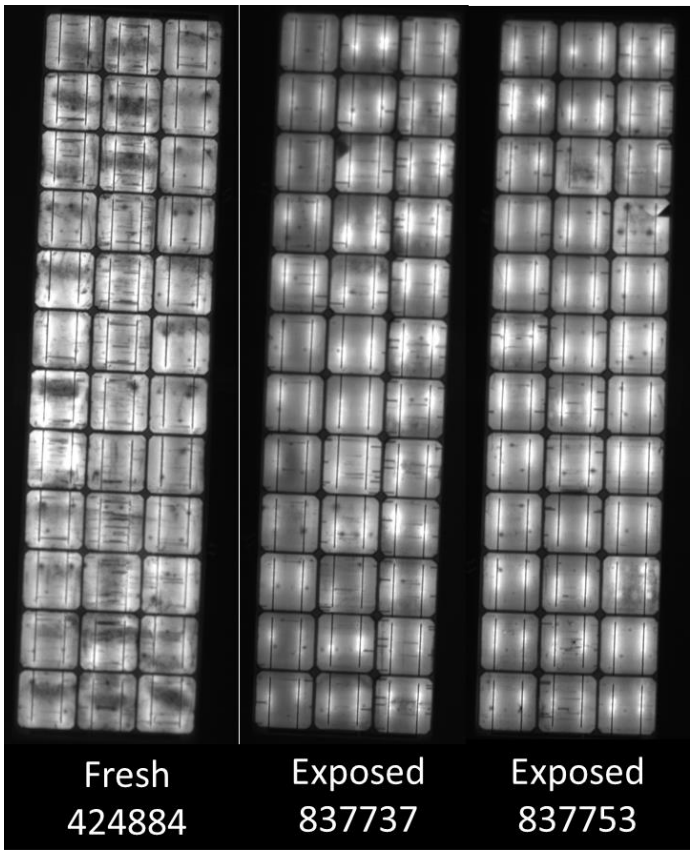

Figure 13: EL of Denver Modules

The conditions under which EL images were taken allow additional information to be interpreted from them. These modules were put under forward bias at a steady current state at 1.33 times the Isc calculated from standardized I-V curves for each module. The darker regions of the cells appear and become more noticeable at higher bias levels which could have indications to specific regions of cells with significant series or shunt resistance issues. Each of these modules experienced approximately equal browning leaving series and shunt resistance issues as the main difference between modules in the best median and worst category. This difference is exemplified in Figures 7-9 EL images. The evenly distributed brightness in the best module shows low solder bond and series resistance issues, however the highly non uniform brightness and greater

amount of bright spots in the EL image shows a large amount of solder bond issues and possible hot spot location along with a significant series resistance increase for the worst modules. When the three environments (Arizona, California and Colorado) for module degradation are compared, the dominant degradation mode for each environment can be seen. For the modules located in Arizona the metal circuit system (interconnect, solder bond and/or cell metallization) issues proved to be a major mode of degradation which is evident through both the EL and IR imaging from the localized dark and bright regions in the EL and localized hot areas in the IR. This form of degradation is most likely a result of high ΔT thermal cycling between night time and day time temperatures, which is unique to Arizona when compared to the other two locations. The SMUD modules from California did not experience the severe amount of the metal circuit system degradation that the Arizona modules did due to the more temperate climate, however due to extended field exposure (18 years in Arizona vs. 28 years in California) and to the increased humidity present in California the browning of these modules was much more extensive. Because Denver is milder temperature wise than Arizona and not as humid as California the exposed modules from Denver proved to be the least degraded after a field exposure of 20 years. These images show examples of module performance for the three locations. The rest of the IR and EL images can be found in Appendix A.

1.3.3 Effect of Series Resistance and Browning on Performance

The last ten points of each I-V curve at near Voc were plotted and the inverse of the slope was taken to determine the series resistance (Rs) for two best, one median, one worst modules and the fresh module. A correlation plot, Figure 14, was then made by plotting

all the I-V parameters versus Rs. Fill factor was the most affected parameter and is the primary cause for Pmax drop due to increase in series resistance, and then encapsulant browning. The degradation of cell interconnects including solder bonds and/or cell metallization was suspected to be the cause for the series resistance increase. Because this trend is based on the physical properties of a module operation this trend is expected in all environments to varying degrees based off of their series resistance.

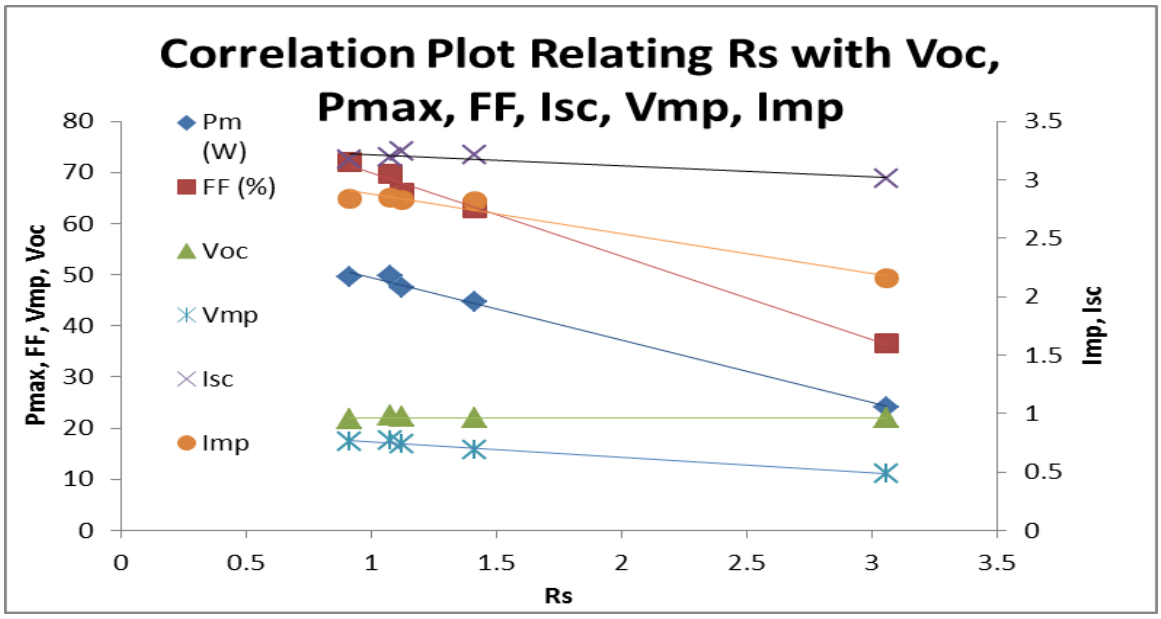

Figure 14: Series Resistance Effect on the Various I-V Parameters.

To quantify the effects of encapsulant browning and oxygen bleaching on module performance, cell-module level quantum efficiency (C-M-QE) and reflectance measurement analysis were performed on all modules from all three locations, Denver, Arizona, and California. Interestingly enough the edges of the cell experience higher reflectance and higher QE than the browned center of the cell. This means that the loss in irradiance caused by browning is greater than the amount of irradiance lost at the edge of the cell through reflectance, and absorbance by the clear encapsulant. Figure 15 shows

both QE curves and reflectance spectra of two spots (center and edge) on cell 7 and cell 2 of the bottom row and middle row (based on the EL image) of field aged module 464137. Since the encapsulant at cell edge is less browned due to oxygen bleaching, both QE and reflectance values are higher than the center spots, which are covered by browned encapsulant, in the low wavelength visible region between 400 and 650 nm.

The peak shown around 400nm is caused by the anti-reflective coating. Due to the properties of AR coating it can only be designed to decrease reflectance to 0 at one point, based on its thickness and chemical properties, which is usually 600nm. The 600nm AR coating thickness is chosen due to the peak power of the solar spectrum around this wavelength [5]. Because all of these measurements are done in the same module it is safe to assume that the composition of the AR coating isn't changing like it might between module designs, instead the amount of light reaching the AR coating, and therefore the cell, is changing due to browning. When the reflectance spectrum of the control module is compared to the reflectance of the aged module a drastic difference can be seen. Due to the degradation of the encapsulant the amount of light reaching the cell in the 400-650nm region of the graph has been reduced as shown in Figure 15. As the degree of degradation of the encapsulant increases the decrease in the reflection peak around 400nm will continue as shown in the reflectance graphs, Figures 20-22 and Figure 15.

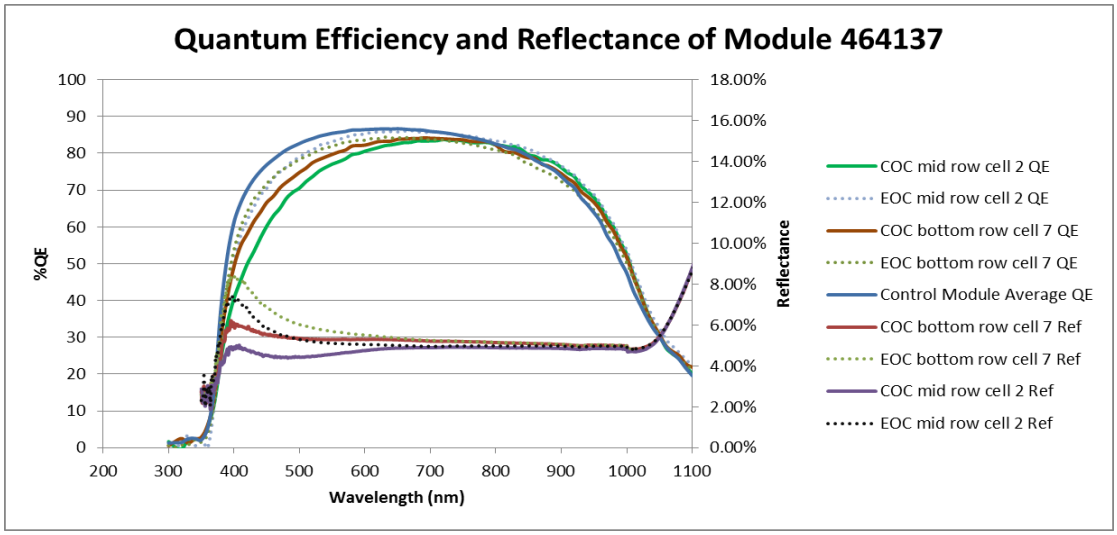

Figure 15: Overlay of Reflectance Measurements and QE Measurements of One Module.

The quantum efficiency of all 9 modules for the Arizona climate were averaged together and compared against the quantum efficiency of the control module. When the average QE of all 9 field aged modules shown in Figure 16 is compared to the QE of module 464137, a best module with lower series resistance, in Figure 15, the effects of series resistance on quantum efficiency can be seen. Series resistance between the best and worst module in the group of 9 aged modules ranged from 9.42 Ohms to 1.06 Ohms, calculated through the Dark I-V method, shown in Figure 18. The series resistance of module 464137 was 1.26 Ohms which is why the QE graph in Figure 15 was mainly affected in the 400-650 nm region due to the browned encapsulant. As the series resistance increases however, losses in QE can be observed throughout the entire spectrum. The difference in QE between the control module and aged modules shows a decrease of 13% over the whole spectrum. The area of the spectrum affected by browned encapsulant (400-650nm) represents 31.25% of the entire spectrum shown in Figure 16. The area of the spectrum affected by mainly series resistance (650-1100nm) represents

56.25% of the entire spectrum. The difference in QE between the aged and control modules, in the browned region (400-650nm region), shows a decrease of 18%. Series resistance also plays a role in the drop noticed in the browned region (400-650nm) and is the reason why this region has a higher difference than the second region. The difference in quantum efficiency between the control module and aged modules QE caused by an increase in series resistance (650-1100) shows a decrease of up to 8% QE depending on the penetration depth of the incident light. If it is assumed that series resistance does not have influence on spectral response, but remains constant throughout the spectrum, then the calculated impact browning has on QE in that region is 10% loss for the Arizona modules; it should be noted that the PRL/Arizona control module was the same type and design as the aged module, however it did have black cells whereas the aged module had blue cells which could lead to a better quantum efficiency for the control module. The same process was applied to both the California modules and Denver modules. The California aged module, when compared to its own control module, showed a 19% loss in QE in the 400-650nm region and a 4% loss in the 650-1100 nm region resulting in a 15% loss in QE due to encapsulant degradation. For the SMUD modules both aged and control modules were the exact same type and color. For the Denver modules the PRL control module was used to compare quantum efficiency losses because after extensive analysis it was concluded that the Denver control module may have cell metallization damages as evidenced in the EL images presented earlier and hence it was not considered as an ideal control module for spot-specific QE measurements. The quantum efficiency loss for the Denver aged modules in the 400-650nm region was 4% for module 837753 and 6% for module 837737. The loss in QE in the 650-1100nm region was 0% and 2% respectively,

which resulted in a resulted in a loss of quantum efficiency of 4% for both modules from Denver. In Figure 17 a visualization of each environment's quantum efficiency is shown.

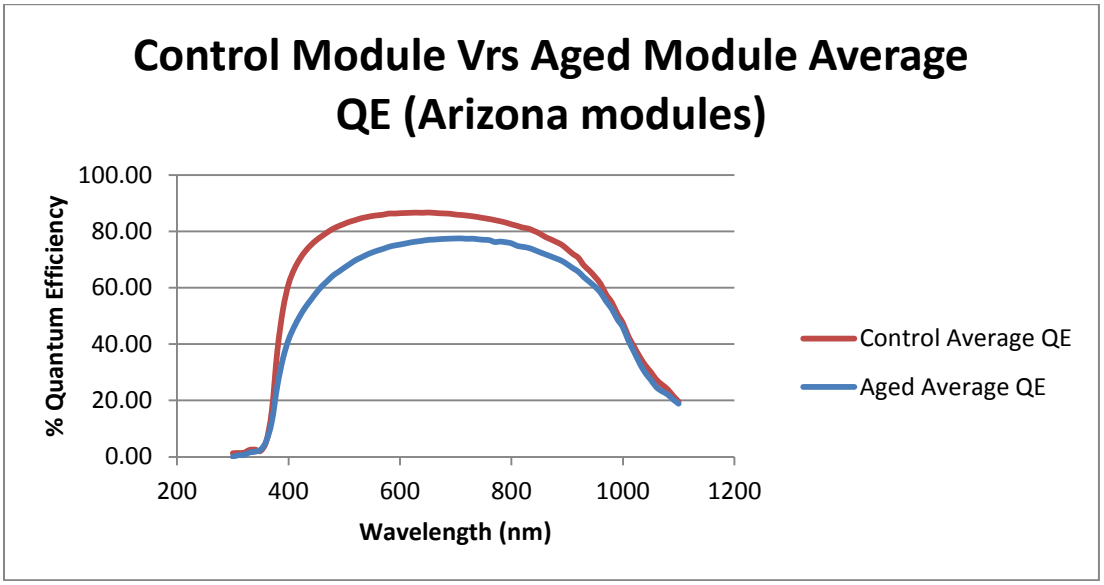

Figure 16: Average QE of all 9 Aged Modules (32 cells total) vs. the Control Module (36 cells)

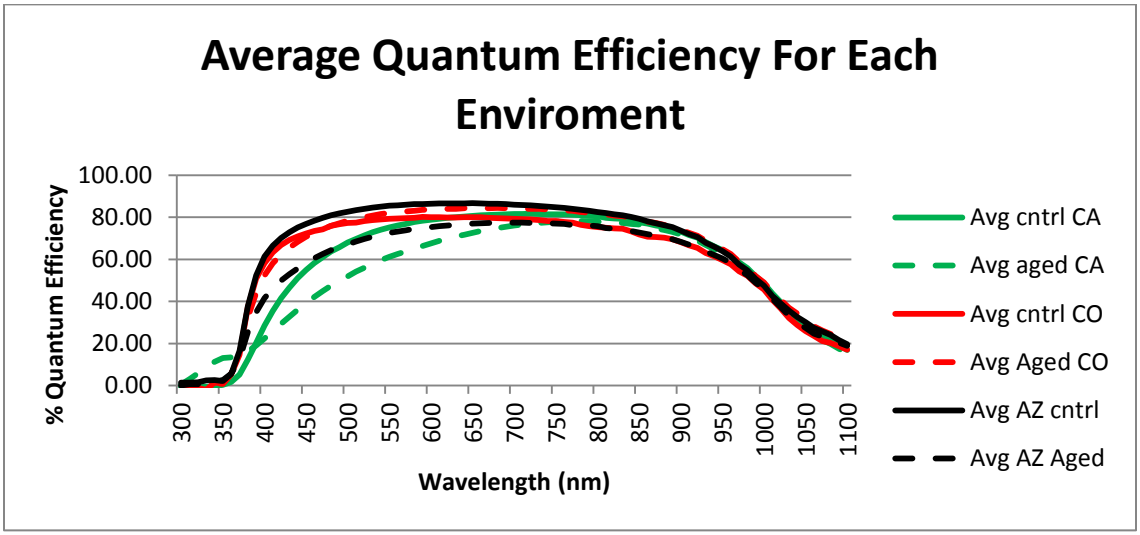

Figure 17: Quantum Efficiency Averages for Each Environment, Both Control (solid lines) and Aged Modules (dashed lines)

Category	Module	Rs (Ohms)
Best	464186	1.16
Best	464185	1.09
Best	464137	1.14
Median	464135	1.67
Median	514207	1.62
Median	514041	1.86
Worst	507968	5.98
Worst	514210	3.29
Worst	514183	9.42

Table 1: Series Resistance for Arizona Modules Calculated Through Dark I-V Method

Method	Module	R_s (Ohms)	Rs Increase
Dark I-V	Control	0.15	27%
	Aged	0.19	
Outdoor I-V	Control	0.13	38%
	Aged	0.18	
Flash I-V	Control	0.12	50%
	Aged	0.18	

Table 2: Series Resistance Values Obtained From Multiple Methods for SMUD Modules

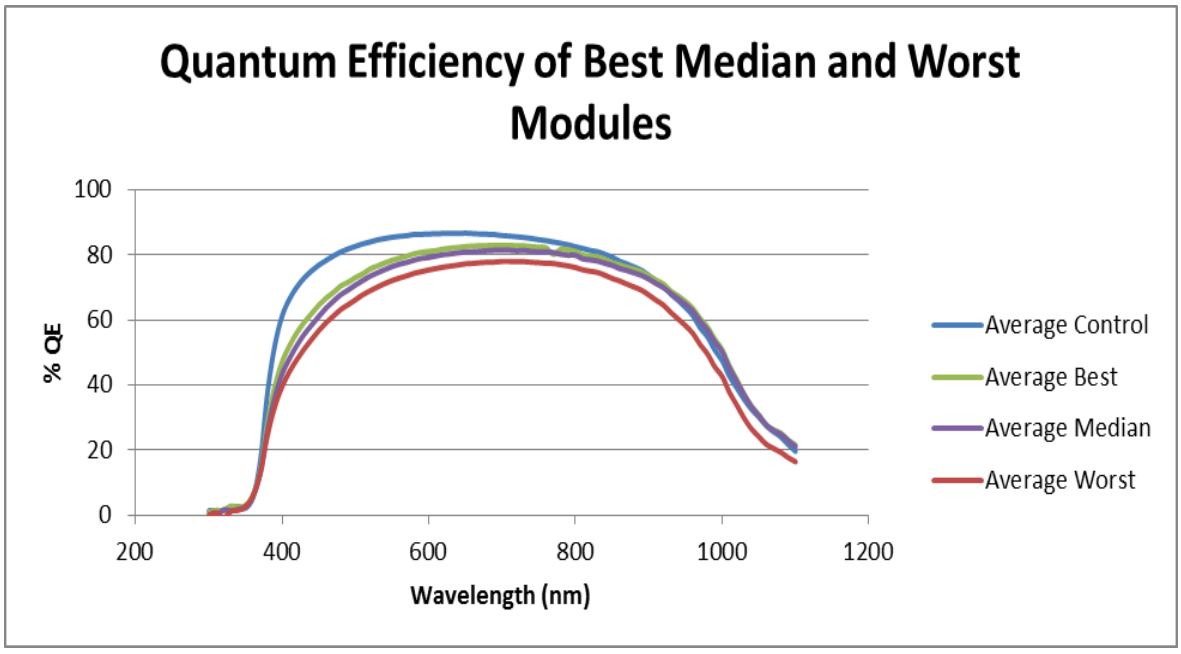

Figure 18: QE of Each Category, Best, Median, and Worst Modules of Arizona

Figure 18 shows the trend series resistance has on the spectral response of a module. The two parts of energy generation in solar modules are first being able to absorb the sunlight and generate electrons, and then being able to collect those electrons. With an increase in series resistance a modules ability to capture all the light generated electrons is hindered resulting in a reduction in QE. As shown in Figure 18 the area referred to as the "series resistance effected region" (650-1100nm) suffers further loss in QE as the series resistance increases from the best to worst category of modules for the Arizona climate. Due to the small number of modules received from the other two environment's this graph could only be produced for the Arizona climate.

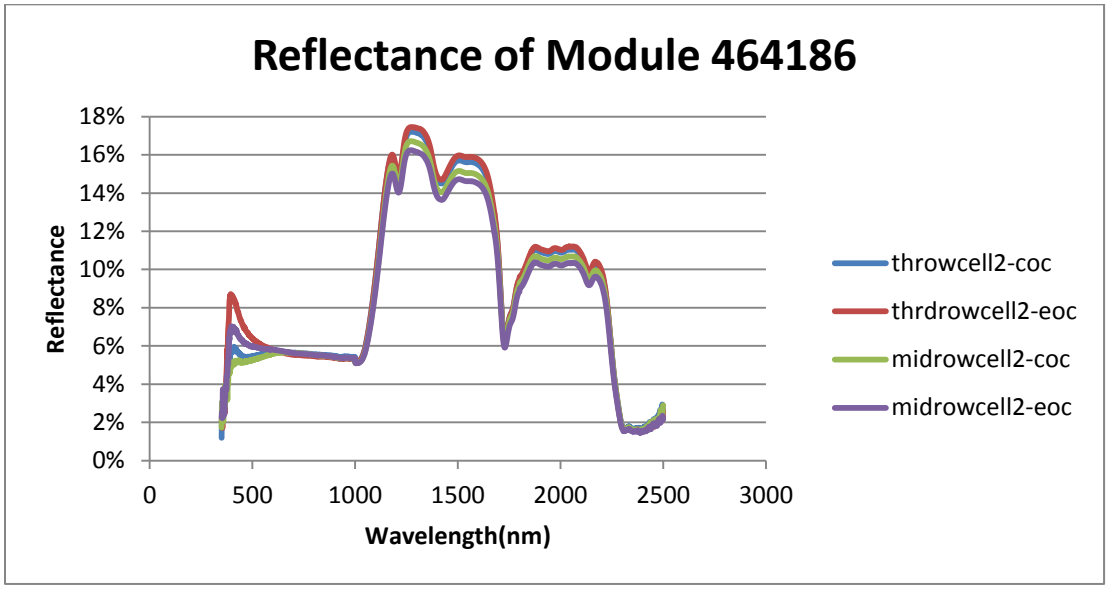

Figure 19: Reflectance of Module 464186, One of the Best Modules in this Study

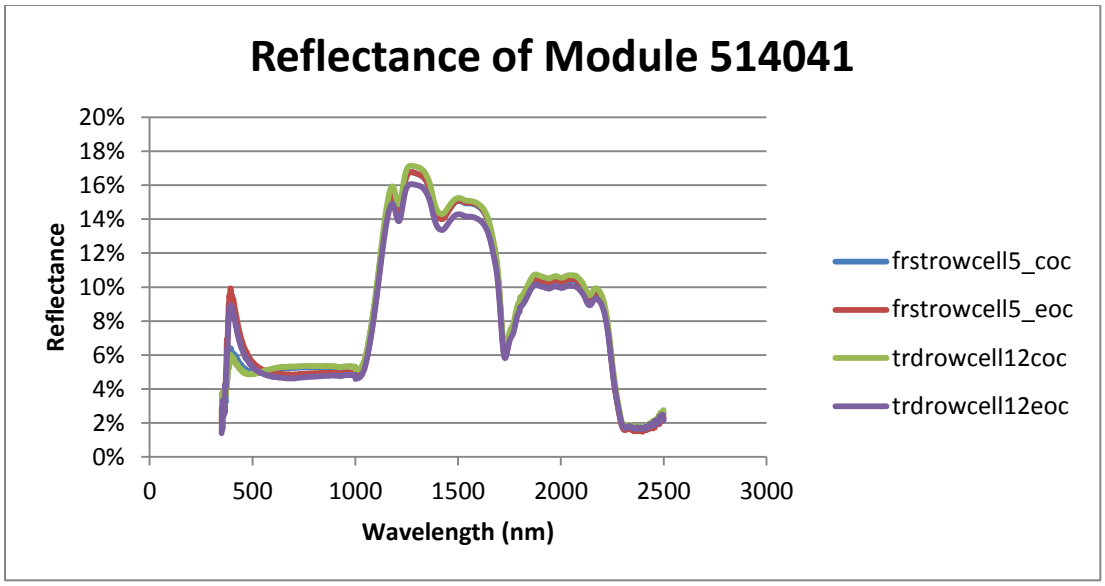

Figure 20: Reflectance of Module 514041, One of the Median Modules in this Study

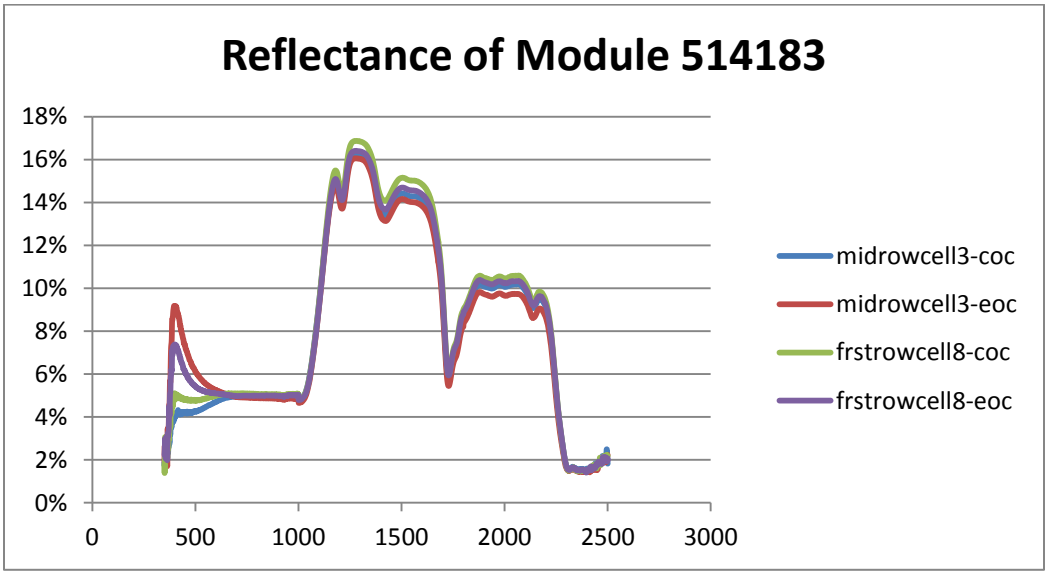

Figure 21: Reflectance of Module 464186, One of the Worst Modules in this Study

While the EVA played a significant role in the loss of spectral response in the 400-650nm region, the rest of the reflectance spectrum showed very little variation between edge and center measurements of aged EVA and between control and aged modules. Figures 19-21 show a module from each category best median and worst from the Arizona climate with two cells selected from each module. There was no change in

peaks or significant reflectance change throughout the rest of the spectrum. In Figure 22 a slight increase in reflectance is shown over the spectrum of a crystalline silicon module, up to 1100nm, for the browned encapsulant measurements when compared to the edge measurements. Only speculation can be made at this point as to the cause of this but this could support the idea that browning is effecting the AR coating itself and not just hindering light transmittance through the encapsulant and into the cell.

Quantum efficiency measurements were taken for every cell of the SMUD aged and control module as well. The QE curves for the control and field aged modules are shown in Figure 22. Much like the Arizona modules browning was suspected to play a major role in the observed drop of power based on the I-V measurements. It is interesting to note that the QE of field aged modules below 390nm is higher than the control module and this may possibly be attributed to the exhausted UV absorber additives in EVA leading to higher QE for the aged module at lower wavelengths.

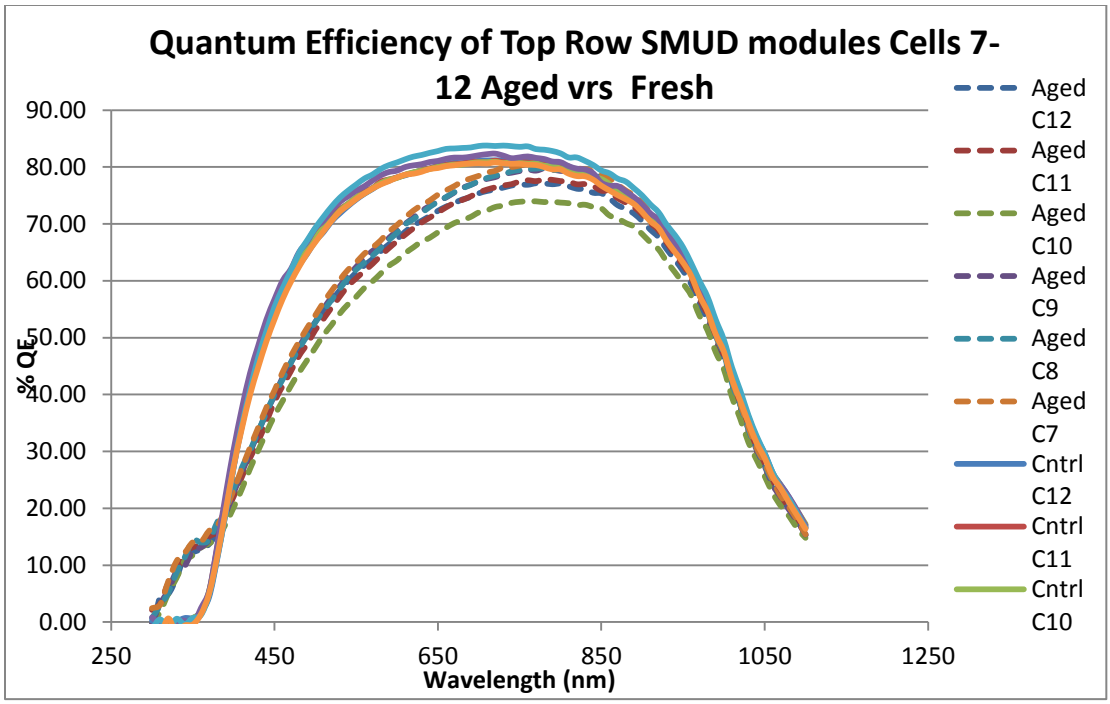

Figure 22 SMUD Aged and Control Module QE Graph

The reflectance spectra obtained for the fresh/control and exposed modules are shown in Figures 23 and 24. The peak seen around 400 nm on the control module, which is caused by the anti-reflective coating, is not there for the aged module which lead to an average reflection loss of 2% from 350-1110nm. The average reflectance from 350 to 700nm for the control module was 5%. The average reflectance of the field aged module from 350-700nm was 2%. The reason for the loss in reflectance in this area is due to the browned encapsulant increased absorption in this region. Due to the encapsulant degradation the anti-reflective coating has either been affected chemically or is not being utilized because the browned EVA is not absorbing the light that would be reflected. Further attention will be given to this point during future research.

When quantum efficiency and reflectance are looked at together an interesting trend is observed. The reflectance for the aged module is lower than the control module

in the 400-650nm region; it means the amount of light being reflected from the control module must be less than the amount of light being absorbed by the browned EVA in the aged module. Due to the severe degradation of the EVA, a large drop in reflectance is evident in the 400-650nm range supporting the QE observations and conclusions presented earlier.

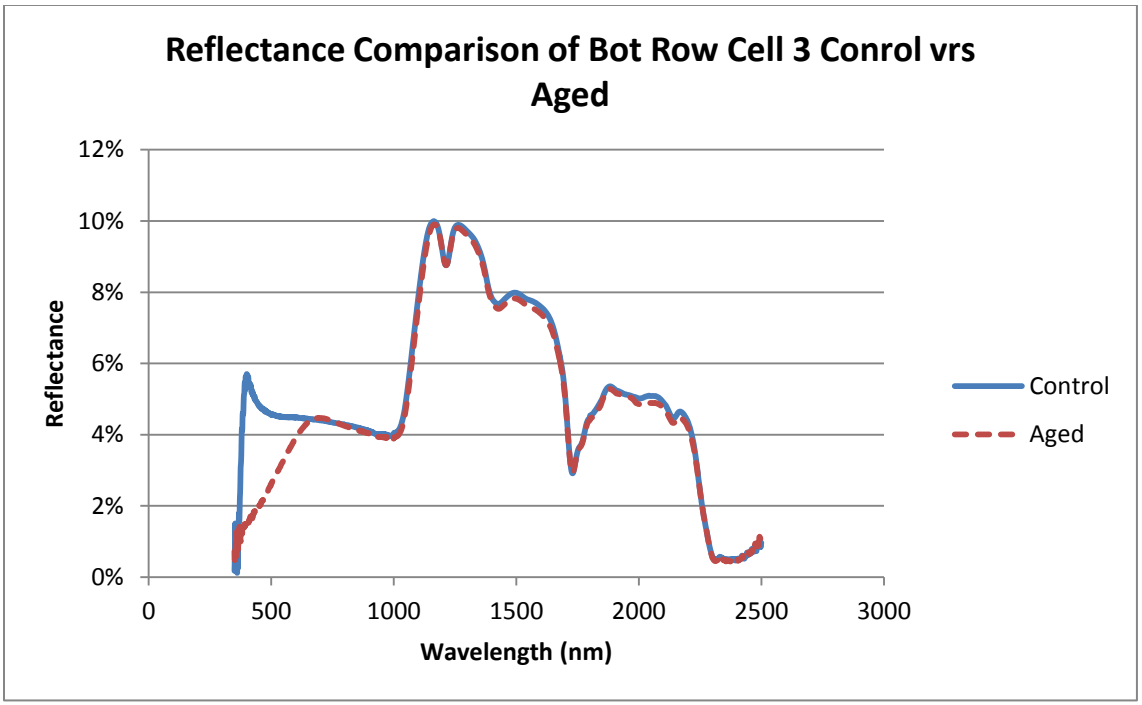

Figure 23: Reflectance Comparison Between Control and Aged SMUD Modules

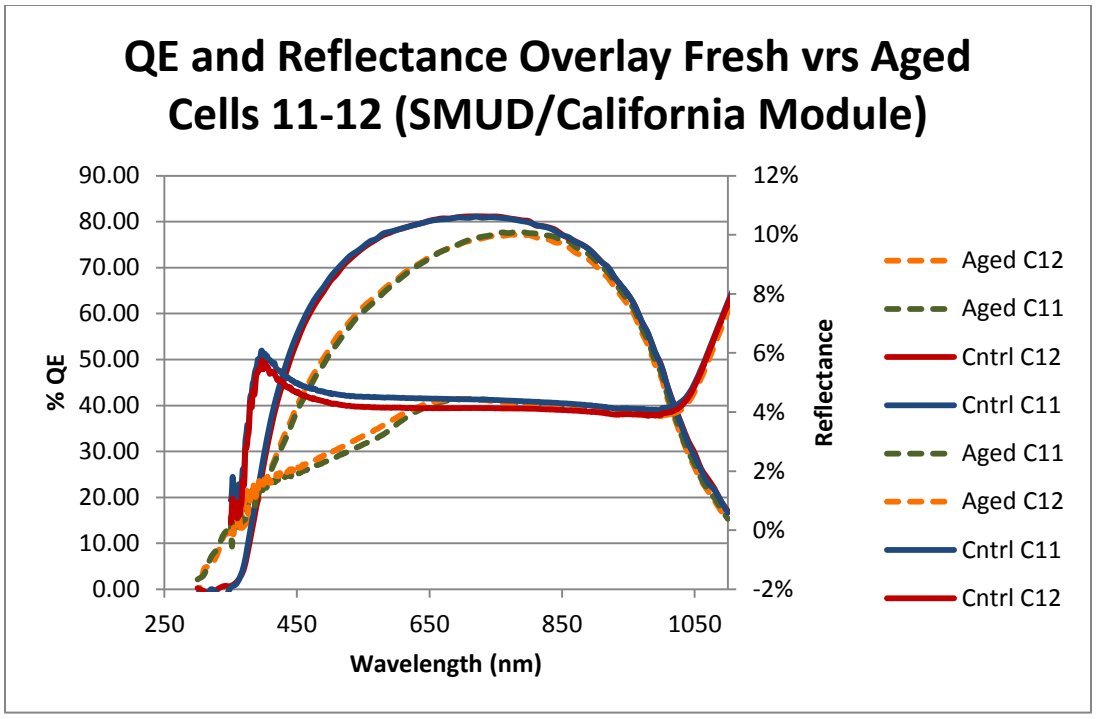

Figure 24: QE and Reflectance Overlay Graph for SMUD/California Module

The change in the peak intensity of the reflectance graphs around 400nm observed between the Arizona and California aged modules could be caused by the current state of the encapsulant degradation level. As the degradation of the encapsulant increased the peak is reduced until a straight line is observed like in the California SMUD modules. When all the Quantum Efficiency graphs from the three locations are compared an interesting correlation can be found. Due to the loss of UV absorber in the SMUD modules a spectral response is seen in the UV region shown in figure 22. However the less browned modules of Arizona and Colorado seem to still have UV absorber present, and therefore have no spectral response on their QE graphs in the UV spectrum. This observation suggests that UV absorber depletion appears to have a positive correlation with encapsulant degradation and browning. Future studies will need to be conducted to look more specifically into this mechanism.

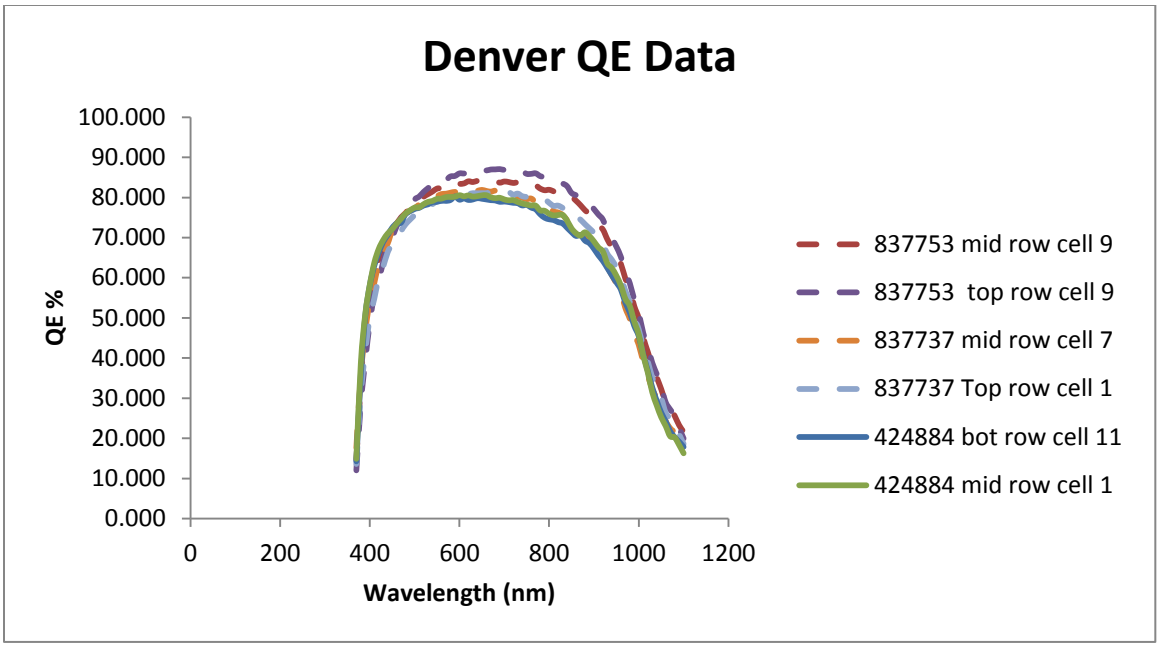

Figure 25: Aged (dashed line) and Control (solid lines) Module Graph of Denver Modules

Figure 25 shows the QE graph of the aged and control modules from Denver. As stated previously it was believed after analysis that the Denver control module may have cell metallization damages as evidenced in the EL images presented earlier and hence it was not considered as an ideal control module for spot-specific QE and this measurements is why the control module 424884 shows a lower QE than the other two aged modules. Figures 26 and 27 show the Denver location module reflectance data. As expected the control module experiences higher reflectance values at both center of cell and edge of cell locations. The main cause of this difference as compared to the other two sites (Arizona and California) was suspected to be very mild extent of browned encapsulant in both of the aged Colorado modules. An interesting difference between the Denver modules and the other two locations was that the reflectance for the Denver modules was different throughout the whole spectrum and not just in the 300-500nm

range..This difference could possibly attributed to the absence of browning and to presence of mild optical decoupling at the cell/encapsulant or glass/encapsualt interface due cold temperature induced delamination. Figure 28 provides an overlaid QE and reflectance plots for one of the aged modules. As evidenced from the absence of QE and reflectance responses below 400nm, Figure 28 clearly indicates that the UV absorber is not lost in the encapsulant of these Colorado aged modules.

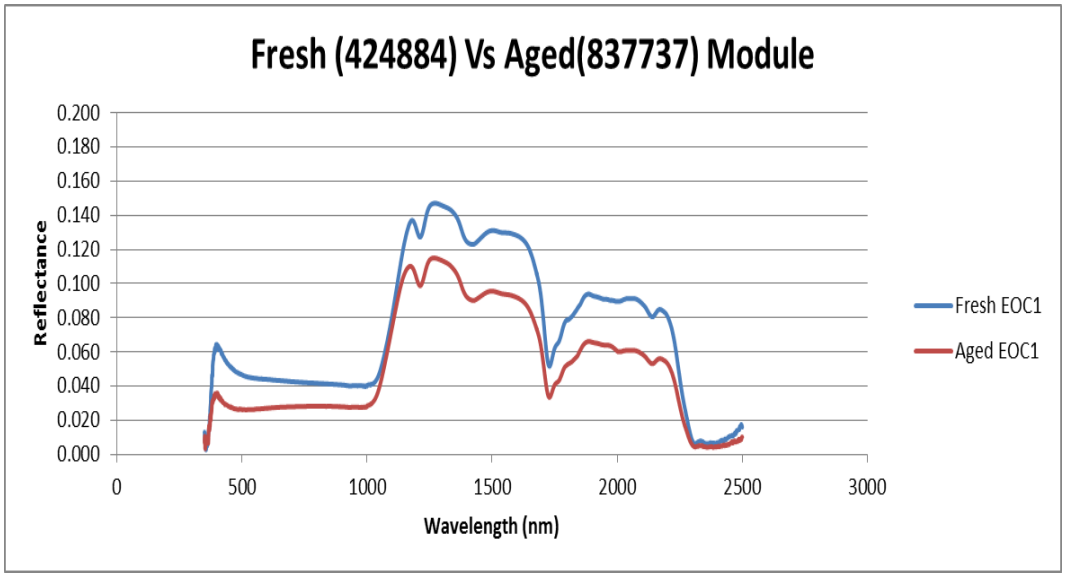

Figure 26: Denver Location Modules Reflectance Spectrum

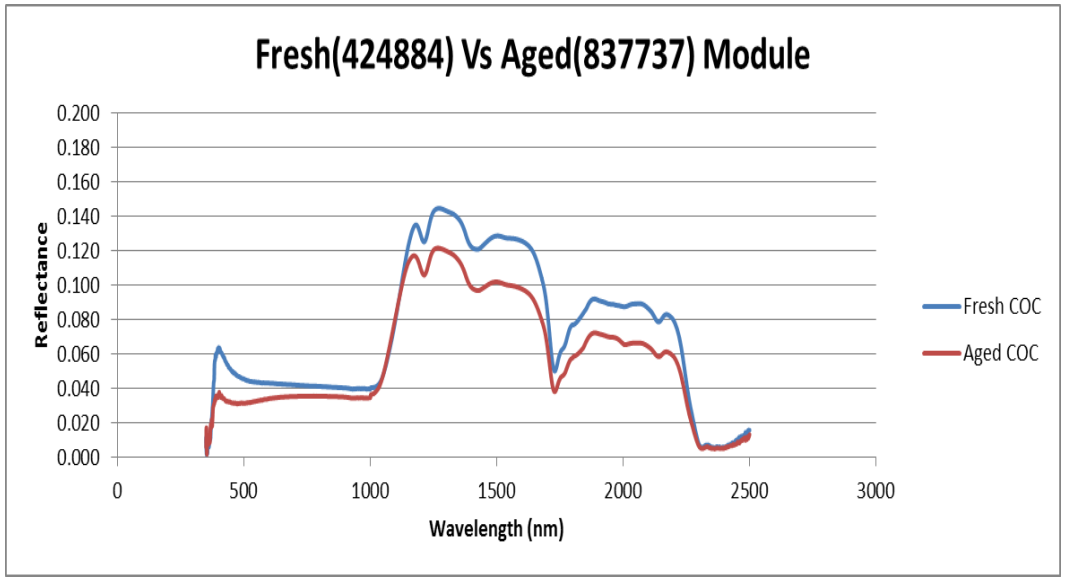

Figure 27: Denver Location Modules Reflectance Spectrum

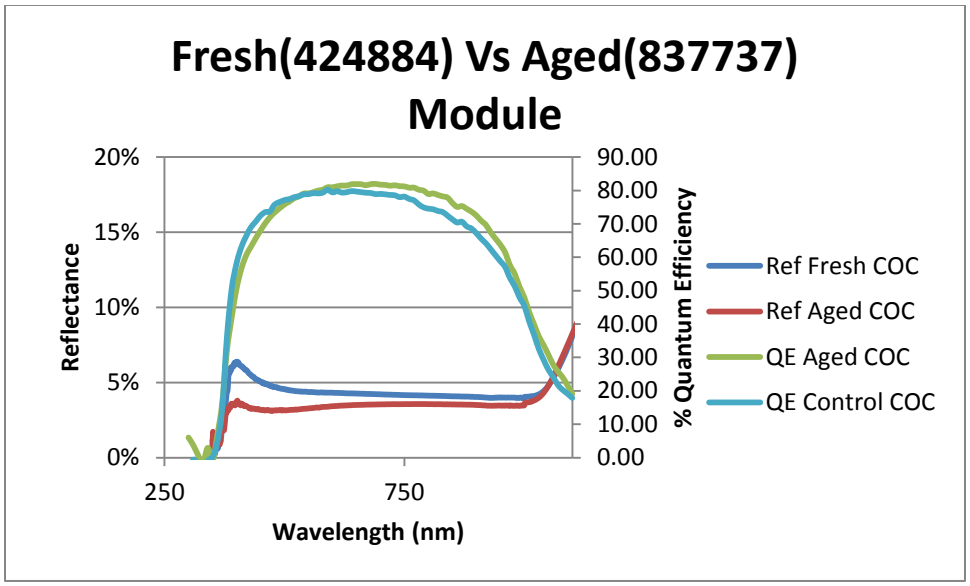

Figure 28: QE and Reflectance Overlay Graph for Aged and Control Colorado Module

CHAPTER 4

CONCLUSION

Major conclusions derived from the non-destructive tests are presented below.

Arizona climate: The average degradation rate of Arizona (hot-dry climate) modules is determined to be 1.16% per year. The two main degradation modes for Arizona climate were encapsulant browning, leading to a loss in current, and increases in series resistance, probably caused by metallization finger deterioration and/or solder bond breakage, leading to fill factor degradation. A new way to quantify the losses caused by browning was introduced using QE and reflectance measurements. Both QE and reflectance analyses indicated the presence or non-exhaustion of UV absorber in the encapsulant even after 18 years of exposure in Arizona climatic condition. Browning was shown to have an effect of module performance mainly in the 450-600nm range. Only the encapsulant area at the cell center excluding cell edges is found to be browned. The power loss in these modules is almost exclusively attributed to the fill factor loss with very little loss from current and no drop at all from Voc. The series resistance of the aged module has been determined to be between 1 ohm and 10 ohms depending module quality (best and worst modules). A direct correlation between fill factor drop and series resistance increase has been established.

California climate: The degradation rate of California (temperate climate) module is determined to be 0.39% per year. The two main degradation modes for California

climate were extensive encapsulant browning, leading to a extensive loss in current, and a small increase in series resistance, probably caused by metallization finger deterioration and/or solder bond breakage, leading to fill factor degradation. Both QE and reflectance analyses indicated the absence or exhaustion of UV absorber in the encapsulant after 28 years of exposure in California climatic condition. Browning was shown to have an effect of module performance mainly in the 450-600nm range. Almost the entire encapsulant area above each cell is found to be browned. The inter-cell spaces were not found to be browned. The hazard warning metal label attached to the backsheet has caused an inter-cell encapsulant discoloration by inhibiting oxygen diffusion through the backsheet. Approximately 62% of power degradation arises from current drop (transmittance loss) and the rest of the power drop primarily arises from FF drop (series resistance increase) with no Voc drop at all. The series resistance of the aged module has been determined to be less than 0.2 ohms indicating that the series resistance increase is not the primary cause for the power degradation of these modules.

Colorado climate: The degradation rate of Colorado (cold/temperate climate) module is determined to be 0.28% per year. No specific or dominant degradation modes have been identified for this site. Both QE and reflectance analyses indicated the presence or non-exhaustion of UV absorber in the encapsulant even after 20 years of exposure in Colorado climatic condition. Very mild browning was observed but it does not have any observable effect on the QE or reflectance curves. An interesting difference between the Denver modules and the modules of Arizona and California was that the reflectance for the Denver exposed modules was lower throughout the whole spectrum and not just in the 300-500nm range as observed in the modules of other two sites. This difference could

possibly attributed to the absence of browning and to presence of mild optical decoupling at the cell/encapsulant or glass/encapsualt interface due cold temperature induced delamination.

REFERENCES

[1] S. V. Janakeeraman, J. Singh, J. Kuitche, J. Mallineni and G. TamizhMani "A Statistical Analysis on the Cell Parameters Responsible for Power Degradation of Fielded PV Modules in a Hot-Dry Climate," IEEE Photovoltaic Specialists Conference, June 2014.

[2] S. Shrestha, J. Mallineni, K. Yedidi, B. Knisely, S. Tatapudi, J. Kuitche, and G. TamizhMani, "Determination of Dominant Failure Modes Using FMECA on the Field Deployed c-Si Modules under Hot-Dry Desert Climate," IEEE Photovoltaic Specialists Conference, June 2014.

[3] D. L. King, M. A. Quintana, J. A. Kratochvil, D. E. Ellibee, and B. R. Hansen, "Photovoltaic Module Performance and Durability Following Long-Term Field Exposure," Progress in Photovoltaics: Research and Applications,8, 241–256, 2000.

[4] B. Knisely, J. Kuitche, G. TamizhMani, A. Korostyshevsky and H. Field, "Non-Intrusive Cell Quantum Efficiency Measurements of Accelerated Stress Tested Photovoltaic Modules," IEEE Photovoltaic Specialists Conference, June 2014.

[5] Pveducation.org, 'Anti-Reflection Coatings | PVEducation', 2015.[Online].Available: http://pveducation.org/pvcdrom/design/anti-reflection-coatings.[Accessed:13-May-2015].

PART 2: DESTRUCTIVE ANALYSIS ON FIELD AGED MODULES

CHAPTER 1

INTRODUCTION

This is a two-part thesis. The non-destructive test results and analysis are presented in Part 1 and destructive test results and analysis are presented in this part, Part 2.

2.1.1 Background

In order to continue dropping the price of solar modules down to goals and targets set by committees a large number of module manufacturers are currently using less or new materials in the design of a module. This includes making PV cell wafers and metallization thinner and . Because of this issue, encapsulants stability and protection are becoming an even more vital part of PV modules designs. As a module ages in the field and is exposed to a variety of environmental factors such as humidity, UV light, and temperature it degrades which can lead to changes in both the chemical and physical properties of the encapsulant. These changes affect both the performance of a module and the protection of the PV cells within a module. In order to increase a modules performance, reliability, and durability over its effective lifetime more understanding is needed in the field of PV module encapsulants and other polymeric materials in the module.

2.1.2 Scope of Work

This part of the thesis goes into detail on some aspects of encapsulant degradation. By investigating the encapsulants state after field exposure from modules in California and Arizona new findings can be made in its degradation mechanism and the key factors that contribute to it.

2.1.3 Literature Review

Much effort has been put into understanding Ethylene Vinyl Acetates (EVA) degradation causes and mechanisms. As a result and combination of UV, and Temperature, exposure EVA is thought to degrade fielded modules through Norrish reactions [6]. These degradation mechanisms, discussed in more detail later on, along with the presence and degradation of UV absorbers result in formation of chromophores in EVA commonly known as "browned EVA" [6]. Other research done by Shaungjun Chen, Jun Zhang, and Jun Su suggest the importance of a third environmental factor, humidity [7]. The importance of humidity on lowering the activation energy of EVA degradation, or increasing the rate of degradation has been supported by many other researchers including F.J. Pern and A.W. Czanderna [8]. However the exact role humidity plays in increasing the degradation rate remains unclear. Below is the composition and proposed degradation scheme of EVA based off of F.J Pern's publication. It should be noted that while the degradation scheme shown in figure 29 does occur in a module, it does not occur kinetically high enough to present significant causes of EVA browning. This is due to the randomness in which the copolymer is placed into the backbone. In order to become a chromophore long attenuated strands of more than 6 C=C bonds must be created and the vinyl acetate only makes up 27-33% of an encapsulants weight resulting in a very unlikely chance that more than 6 vinyl acetate

copolymer segments will be found next to each other. The more important aspect of this scheme is the acetic acid production. Very little acetic acid is required to cause a drop in pH in a localized environment. Acetic acid could play a role in catalyzing other degradation reactions within the module, such as solder bond damage or cell shunting.

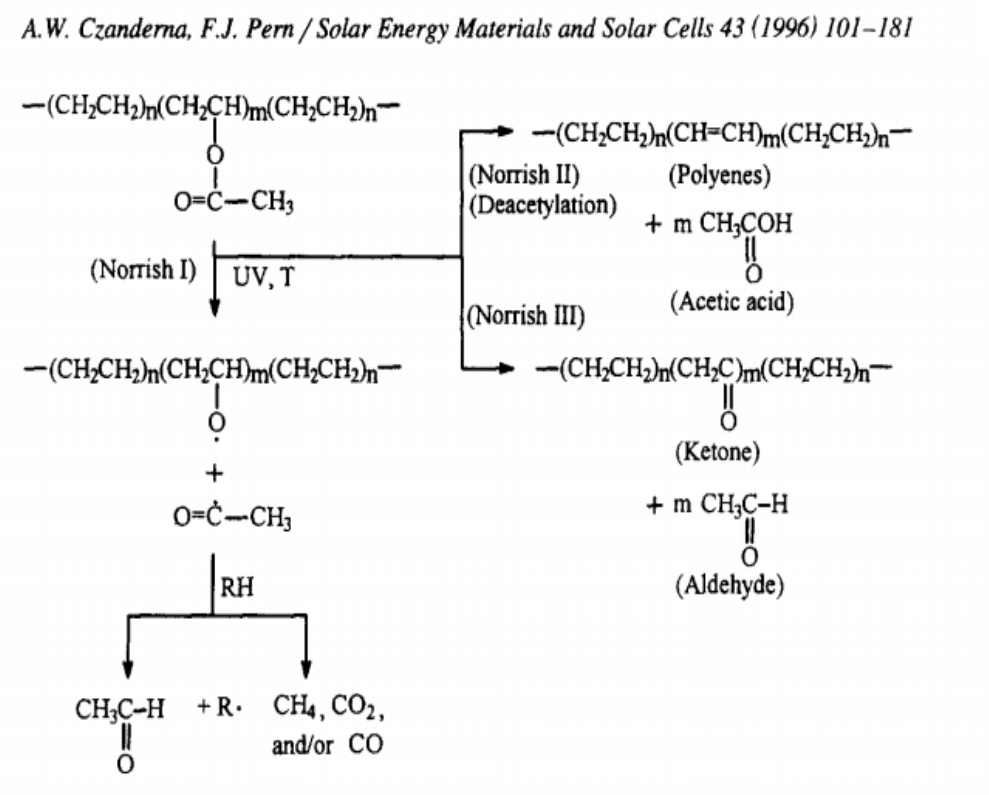

Figure 29: Proposed Degradation Scheme of Encapsulants [6]

CHAPTER 2

METHODOLOGY

2.2.1 Sample Collection, Storage, and Preparation

The samples from both control and aged samples were cut using a diamond wheel dremel tool attachment. After the encapsulant pieces were physically separated from the cut samples using a knife, they were wrapped in an aluminum foil and placed in a plastic

bag. Plastic bags were used to prevent environmental contamination, and aluminum foil was used to prevent exposure to erucamide, a commonly used anti-static material in plastic bags. Figures 30 through 32 show the photographs taken during sample extraction. To understand the degradation mechanisms of EVA, the extracted EVA samples were subjected to DSC (-60^{o}C to 250^{o}C), TGA (room temperature to 600^{o}C) and FTIR (from 4000 cm^{-1} to 700 cm^{-1}) characterizations. The results obtained from these characterizations are presented in the following sub-sections.

Figure 30: Diamond Dremel Tool Cutting Out the Center Part of a Cell

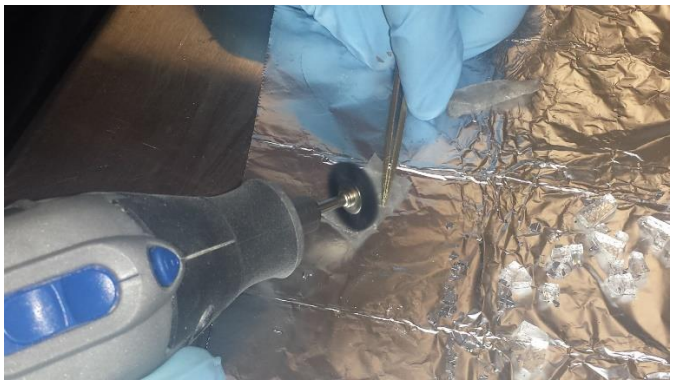

Figure 31: Dremel Tool Plastic Brush Cleaning the Extracted EVA layer

Figure 32: Photograph of a Module With Center Part of a Cell Removed from the Laminate

2.2.2 Fourier Transform Infrared Spectroscopy (FTIR)

FTIR was performed using an Agilent 4300 handheld FTIR instrument. Results were verified by rocky mountain laboratories. Samples of Removed EVA were placed onto the Mounting Structure shown below and scanned using a Diamond ATR attachment.

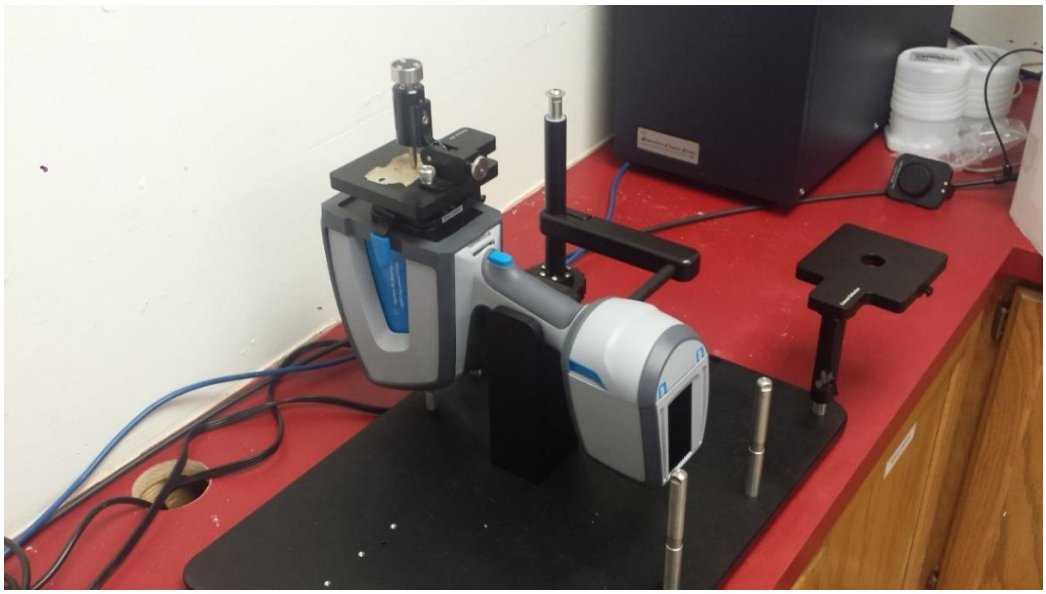

Figure 33: Hand Held FTIR Setup

2.2.3 Differential Scanning Calorimetry (DSC)

The DSC Q20 from TA instruments, shown below, was used to perform all DSC measurements. Small hole punch samples were placed into sample holders for each run performed. The sample holders shown in figure, were placed into an air tight chamber and a run sequence was chosen based off of the desired analysis of the experiment. Various run sequences were performed based off of current standards and conditions required to test for a variety of physical states such as melting transition, crystallization temperature, glass transition state, and degree of curing calculations.

The various run sequences can be found described below with their respective calculation.

Two rounds of DSC were run on the encapsulant samples obtained from both the control and the aged modules.

- Cycle1: Ramp down to -60^{o}C from room temperature
- Cycle2: Ramp up to 250^{o}C @ 10^{o}C/min
- Cycle3: Ramp down to -60^{o}C @ 10^{o}C/min
- Cycle4: Ramp up to 250^{o}C @ 10^{o}C/min

Curing DSC cycle and analysis were performed according to IEC 62755
Run parameter:

- Initial temperature: 20 C
- Ramp to 100 C at 10C/min
- Ramp to -20 C at 10 C/min
- Ramp to 225 C at 10 C/min

Figure 34: DSC and Cooling Tower Attachment Used for DSC Analysis

Figure 35: Hermetically Sealed pan (left) with its Lid (right)

2.2.4 Thermogravimetric Analysis (TGA)

TGA was run the Q50 from TA instruments, in a nitrogen atmosphere. All samples were run from room temperature to approximately 600°C. Multiple heating rates were used to calculate activation energy according to ASTM standard 1641-04. In addition to activation energy calculations TGA was used for % vinyl acetate determination. This was done to understand the effect of side chain removal, or lack thereof, on encapsulant browning.

CHAPTER 3

RESULTS AND DISCUSSION

2.3.1 Chemical and Physical Encapsulant Characterization

Figure 36 and Table 3 show the typical FTIR spectra of dry and hydrated EVA [9]. The potential degradation pathway of EVA due to heat and UV is shown in Figure 29 . FTIR spectra shown in Figures 37-39 and Table 4 for the EVA of aged SMUD module indicate the absence of hydrolysis (broad peak at 3200-3600 cm^{-1}) but presence / formation of polyenic chromophores (1641 cm^{-1}, 1545 cm^{-1}). Based on the small (may be considered not significant) broad peak around 1600 cm^{-1}, UV-Vis-NIR reflectance spectra between 400 and 650 nm and the spectral/QE response between 400 and 650 nm, it may be possible to indicate that the polyenic chromophores have been formed only for the front-EVA of the aged sample due to heat and UV, but not for the control samples (no UV or heat) and the back-EVA of the aged sample (no UV). To confirm this argument, this study needs to be extended with additional number of samples from this and other modules which have browned EVA. The acetic acid formation due to deacetylation (Norrish II reaction pathway) may lead to corrosion of metallization, busbars, solder bonds, cell interconnects and string inter connects. Corrosion of these components is expected to increase the series resistance of the cell leading to fill factor drop (see Table and Table1 and 2). Figures 40 and 41 are the FTIR graphs of the Arizona aged modules. These modules show simliar results as the SMUD modules.

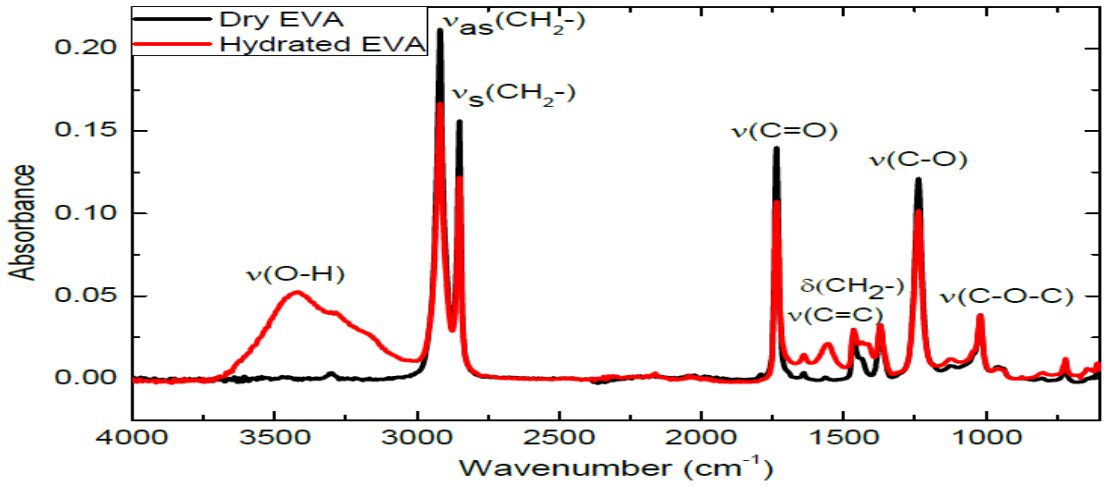

Figure 36: Typical FTIR Spectra of Dry and Hydrated EVA [9]

Wavenumber (cm^{-1})	**Vibration Mode**
3200-3600	Hydroxyl stretching O-H
2918	Asymmetric vibration of –CH2
2849	Symmetric vibration of –CH2
1735	Ketone (C=O) Stretching
1641, 1545	Polyene (C=C) vibration
1464, 1370	-CH2 bending
1235	Ester (C-O) Stretching
1019	Ester (C-O-C) Stretching

Table 3: Typical FTIR Spectra of Dry and Hydrated EVA

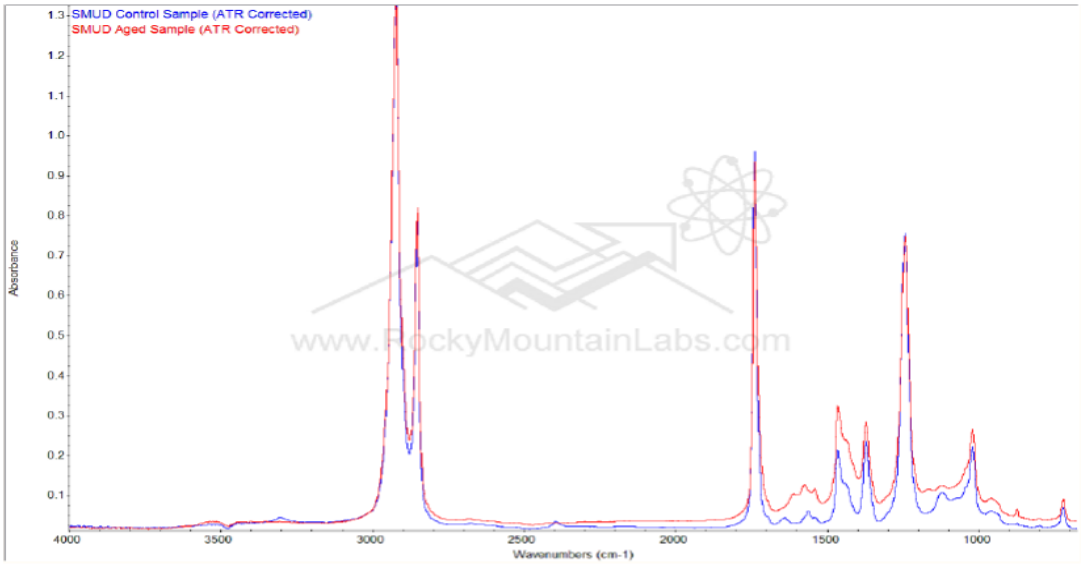

Figure 37: FTIR of Extracted EVA for SMUD Modules Control and Aged

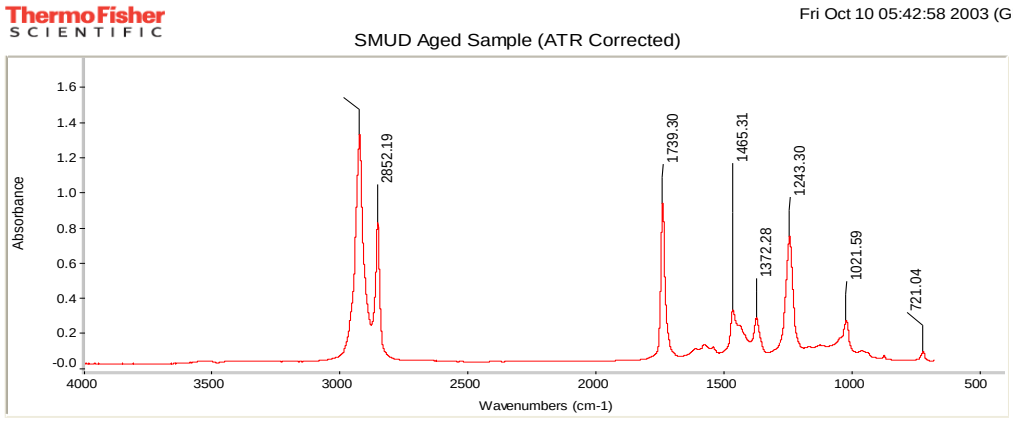

Figure 38: FTIR of EVA of Aged SMUD Modules

Wavenumber (cm^{-1})	Vibration Mode
2923	Asymmetric vibration of –CH2
2852	Symmetric vibration of –CH2
1739	Ketone (C=O) Stretching
1641, 1545	Polyene (C=C) vibration
1465, 1372	-CH2 bending
1243	Ester (C-O) Stretching
1021	Ester (C-O-C) Stretching

Table 4: FTIR Spectra of EVA of Aged SMUD Module

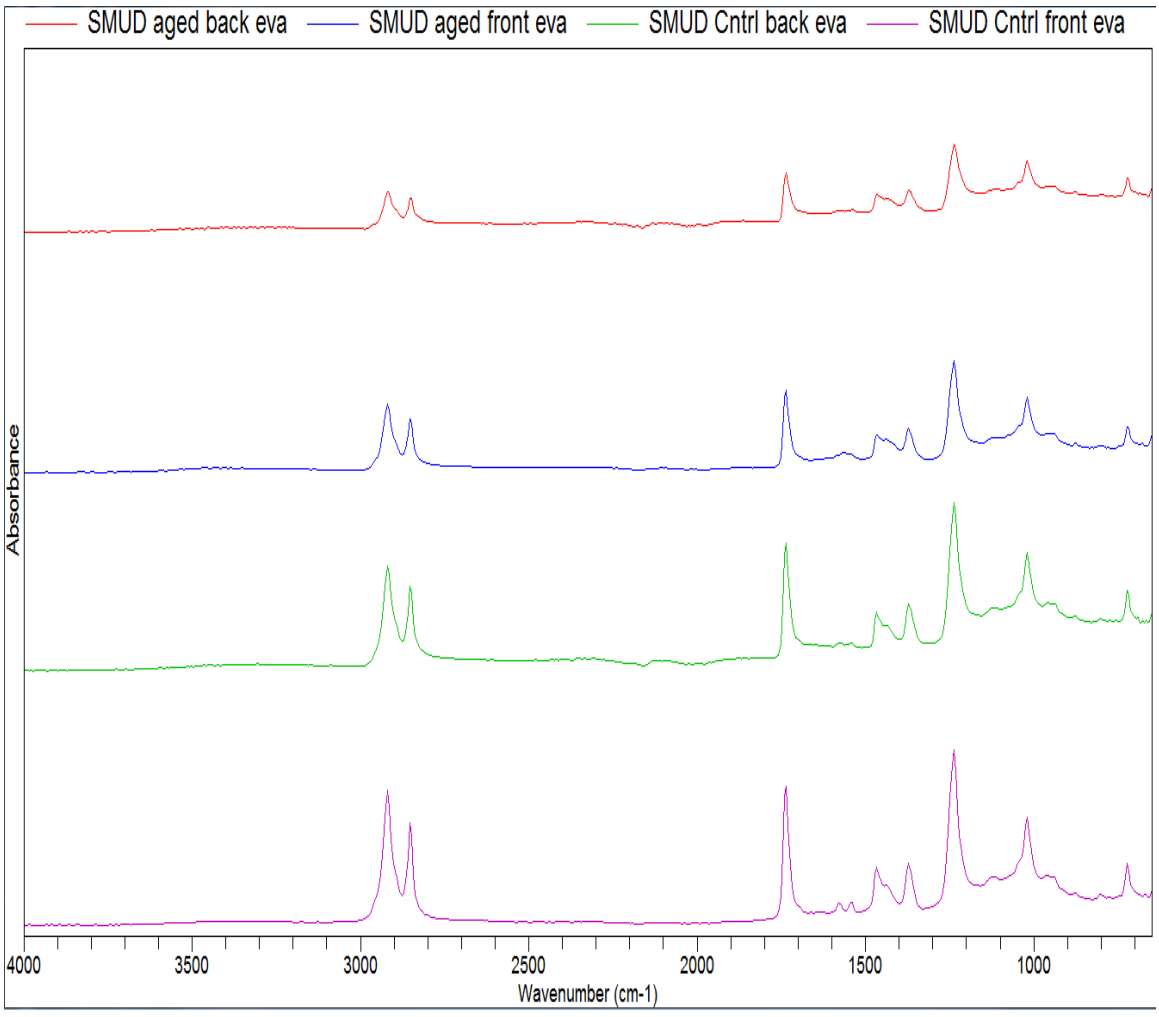

Figure 39: FTIR Graph of SMUD Modules Stacked Display Analysis Performed by PRL

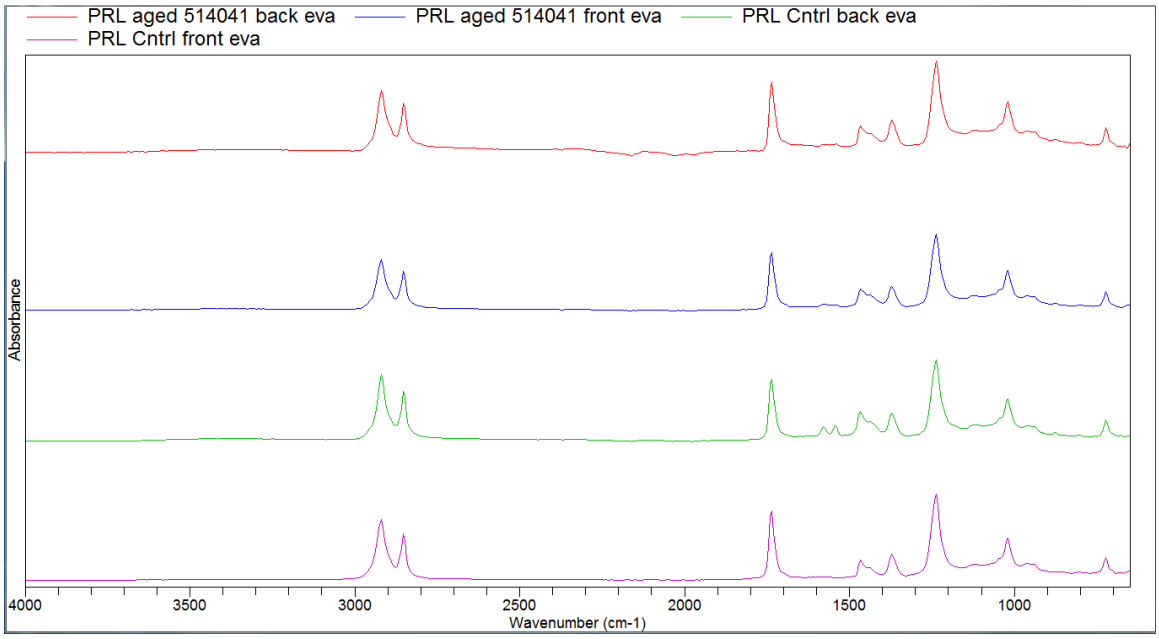

Figure 40: PRL Aged and Control Module FTIR Stacked Display

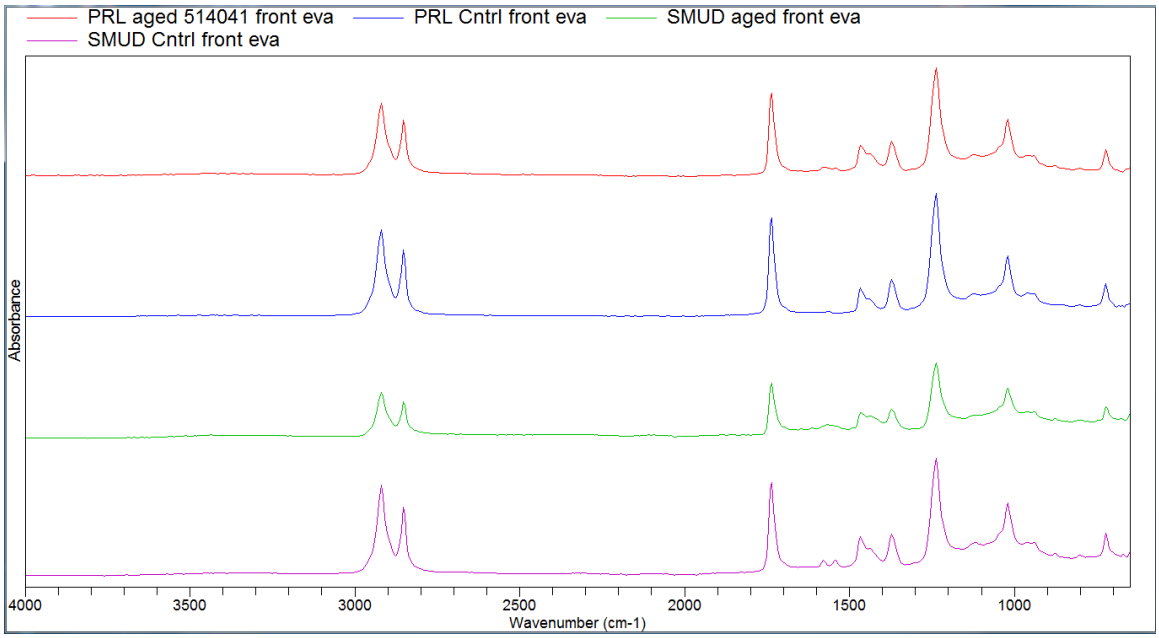

Figure 41: PRL and SMUD Aged and Control Module FTIR Stacked Display

Figures 42 through 45 provide the DSC thermograms for the EVA samples of both control module (never exposed module) and aged modules (exposed for 28 years at the SMUD site). The DSC thermograms were obtained on the samples extracted from the

front side of the cell and back side of the cell. In the aged modules, the front EVA is exposed to all the environmental stresses and UV but with limited access to oxygen and moisture access through the backsheet. On the other hand, the back EVA is exposed to all the environmental stresses except UV but with higher level of access to oxygen and moisture. The two endothermic peaks observed between 50 and 80^{o}C for cycle 2 (before recrystallization) of aged samples (both front- and back-EVA) correspond to the melting of imperfect crystalline phase (first peak) and primary crystalline phase (second peak) of polyethylene. Only one peak appears, after recrystallization, in cycle 4 indicating the disappearance of one of the phases during the previous heating cycle. On the other hand, only one peak, even in cycle 2 before recrystallization, is observed in the control samples for both front- and back-EVA indicating the presence of only one phase (imperfect crystalline) in the material. The exothermic peaks around 35-40^{o}C corresponds to the recrystallization of the samples. Note that the recrystallization peak for the aged front-EVA is very broad as compared to all other three peaks. The broad exothermic peaks observed in the control samples around 180-210^{o}C fore cycle 2 (before recrystallization) are attributed to the curing process of the encapsulant activated by a combination of heat and peroxides in EVA and they disappear in cycle 4 due to consumption of peroxides leading to EVA curing in the previous cycle. These broad exothermic peaks do not appear, even in cycle 2, in the aged samples as peroxide is already consumed for cross linking in the field over 28 years of exposure in the field. The degree of cure can be calculated using a new standard (IEC 62755) which is being developed. These thermograms clearly indicate that the aged samples are fully cross linked. The peaks seen in the control module but not in the aged module around 200 C represent lubersol 101, a

slow curing agent used in PV production. This chemical is known to have correlation to EVA browning and its absence from the aged modules further proves this point.

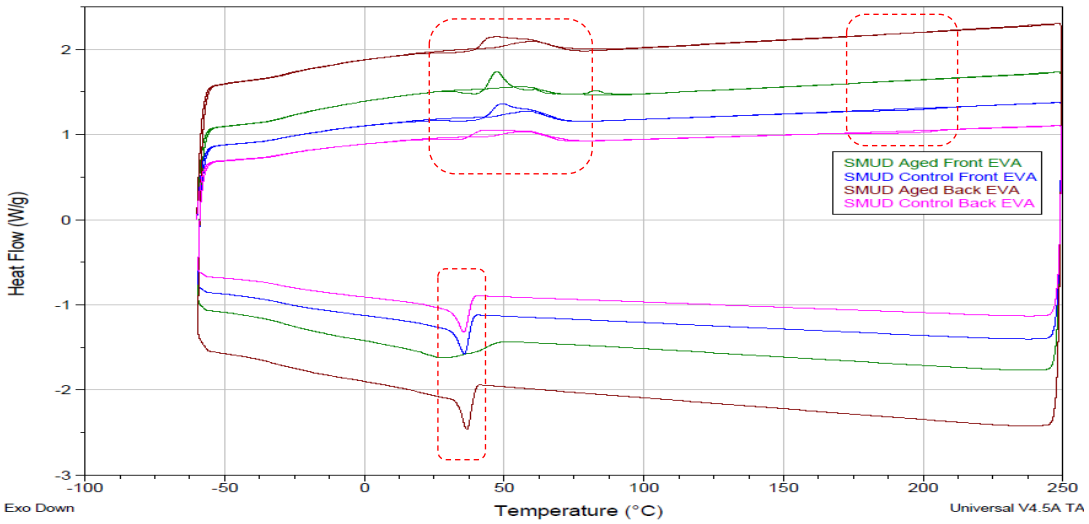

Figure 42. DSC Thermograms for Cycles 2 (heating), 3 (cooling) and 4 (heating)

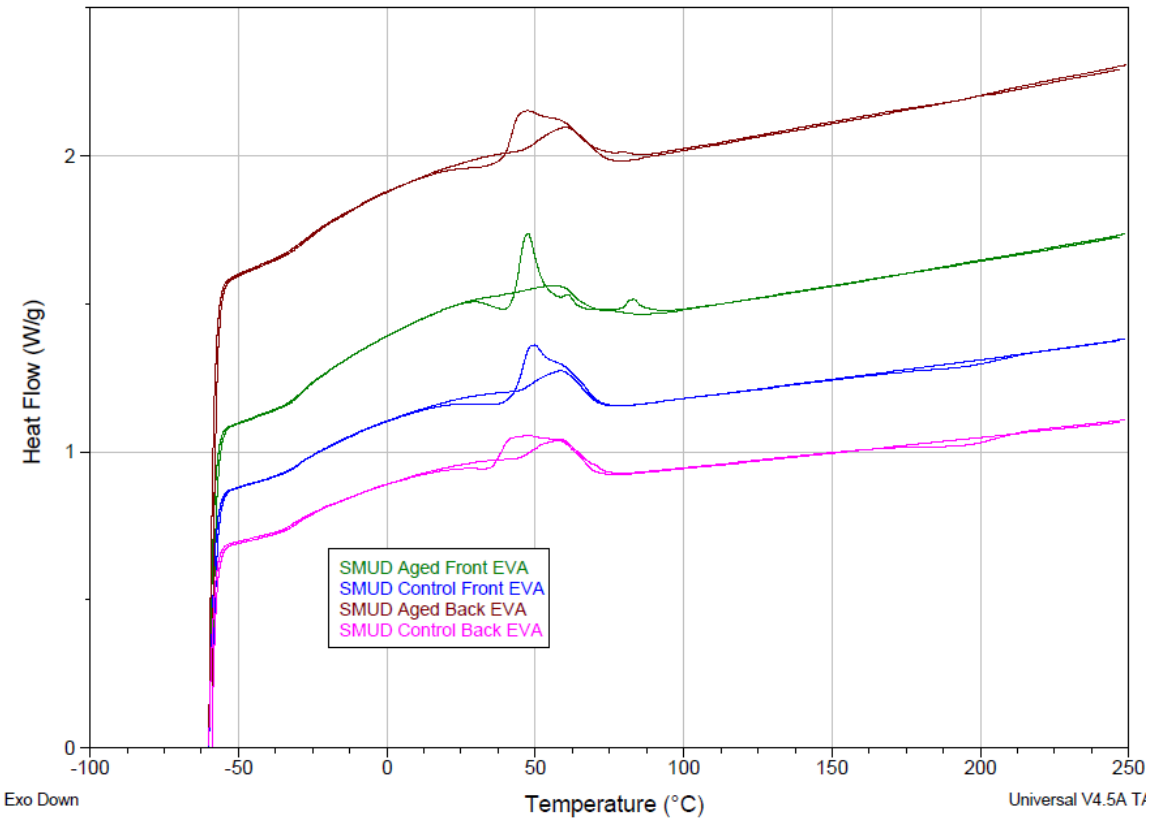

Figure 43: DSC Thermograms for Cycles 2 and 4 SMUD Modules

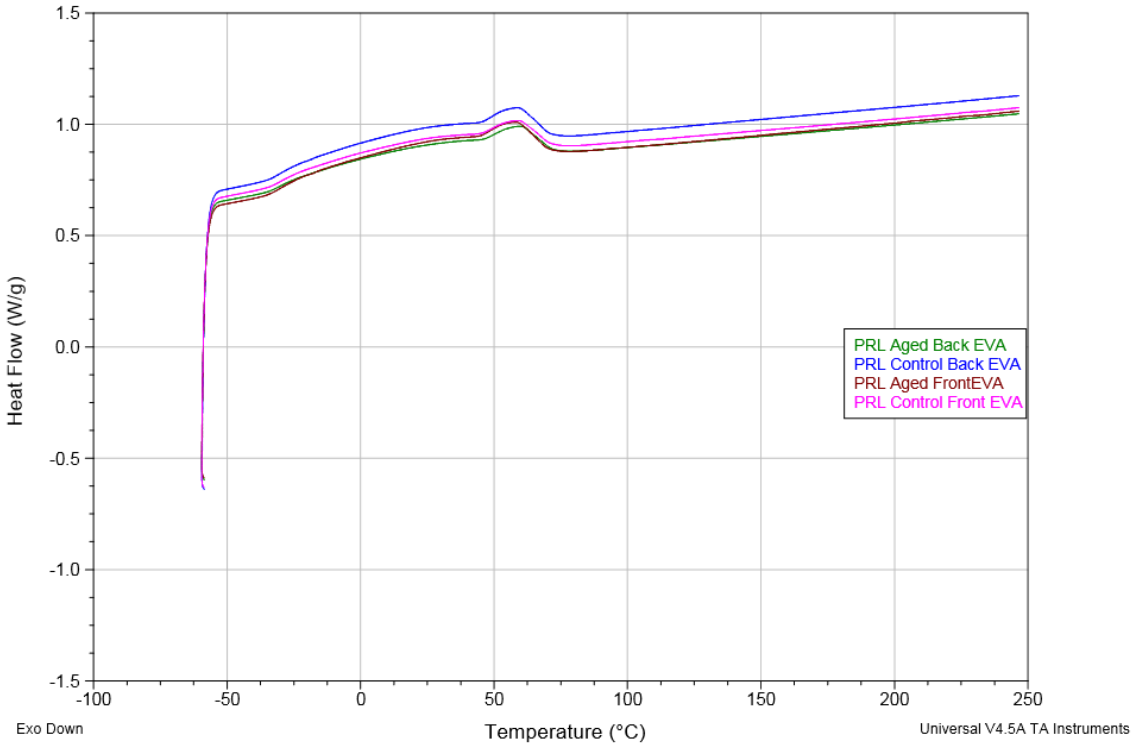

Figure 44: DSC Thermograms for Cycles 2 and 4 PRL Modules

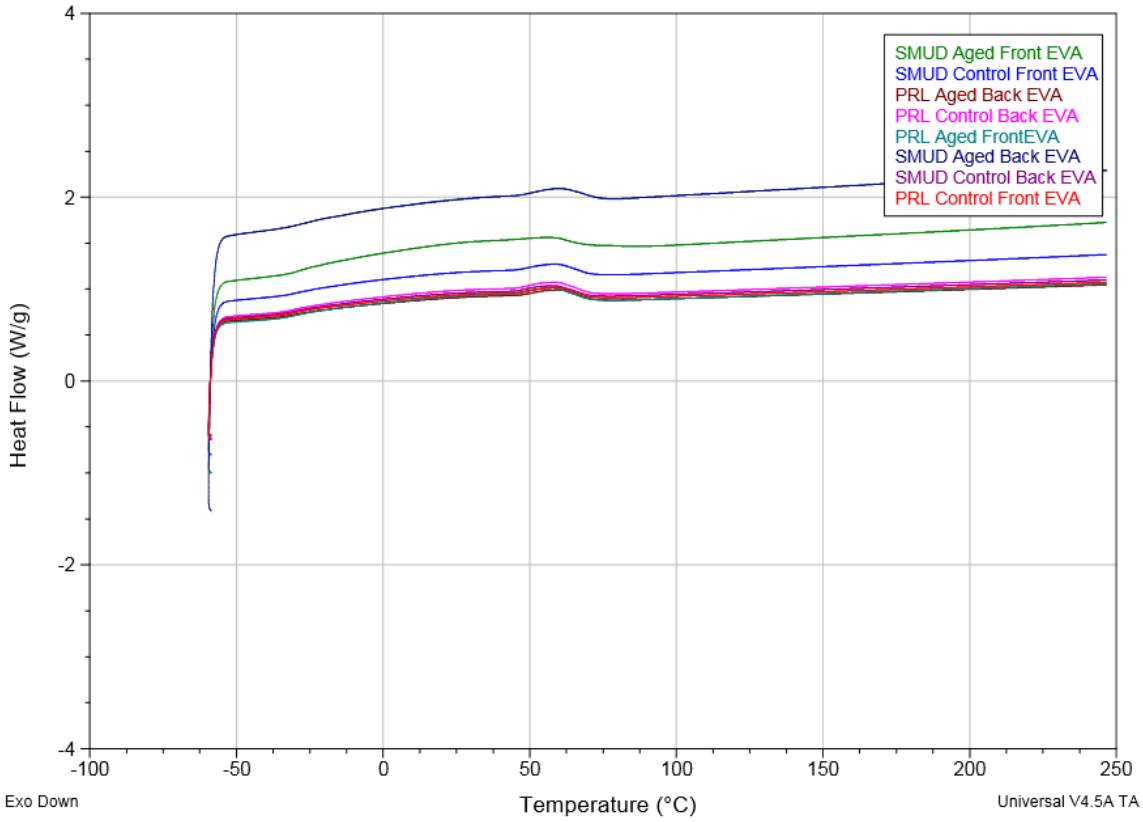

Figure 45: DSC Thermograms for Cycles 2 and 4 All Modules

Figure 46 and 47 provides the TGA thermograms obtained in dry N_2 atmosphere for front-EVA and back-EVA of both control and aged modules. Figure 48 provides the TGA thermograms for the stabilized and cured EVA in dry N_2, O_2, and O_2 saturated with water vapor. Comparison of these thermograms in these two figures indicates that the EVA material in the aged module has not been affected by the reactions caused by oxygen or moisture. Based on the QE, reflectance, FTIR and TGA studies, it may be possible to conclude that the observed EVA discoloration is apparently caused by heat and UV without significant influence from atmospheric oxygen and humidity.

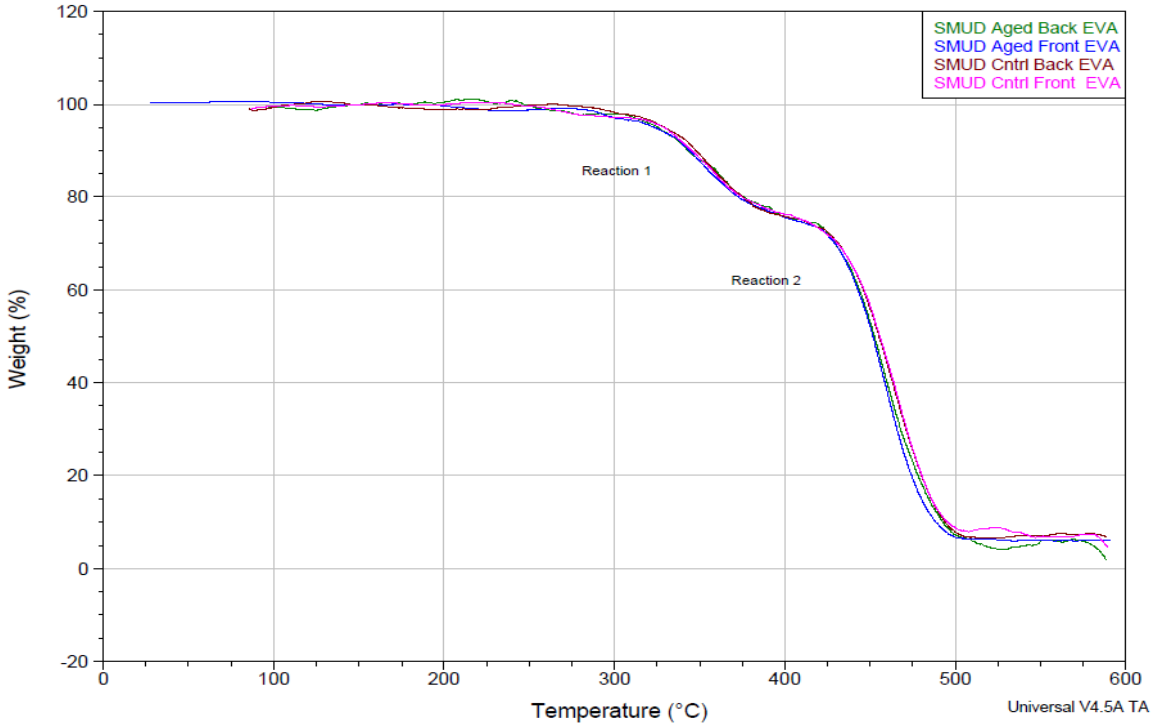

Figure 46: TGA Thermograms of Aged and Control Modules of SMUD

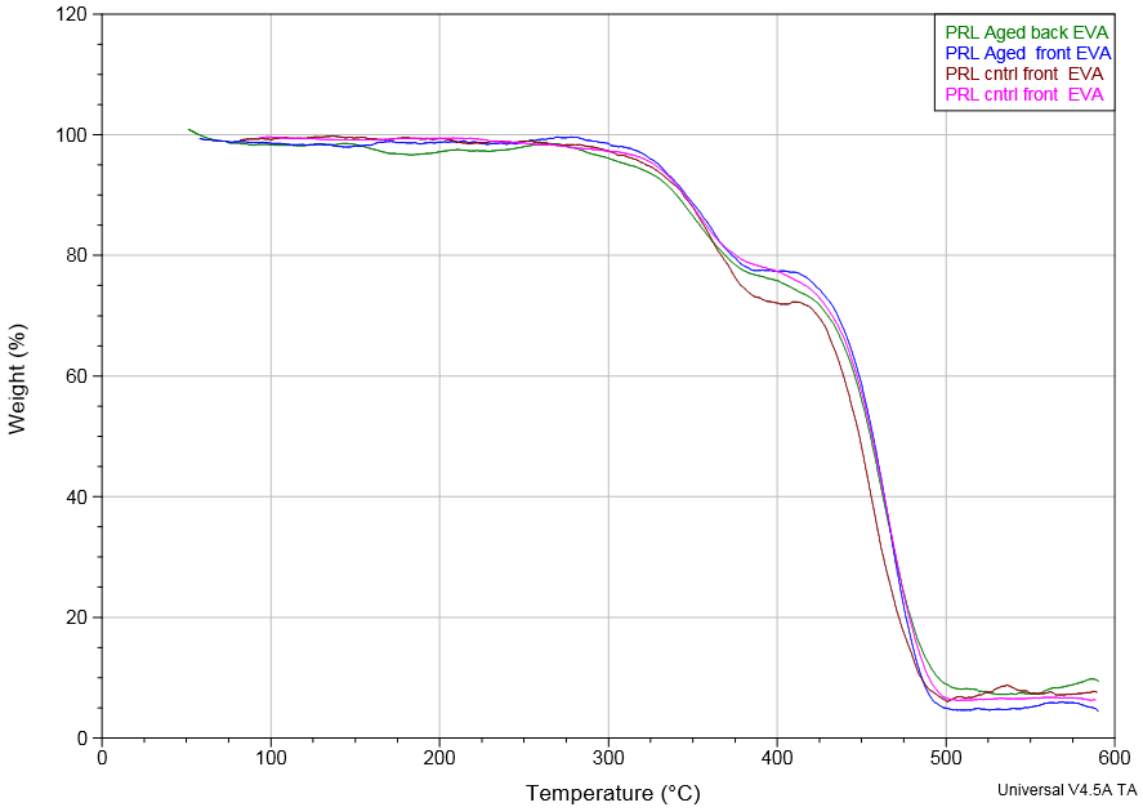

Figure 47: TGA Thermograms of Aged and Control Modules of PRL/Arizona Aged Modules

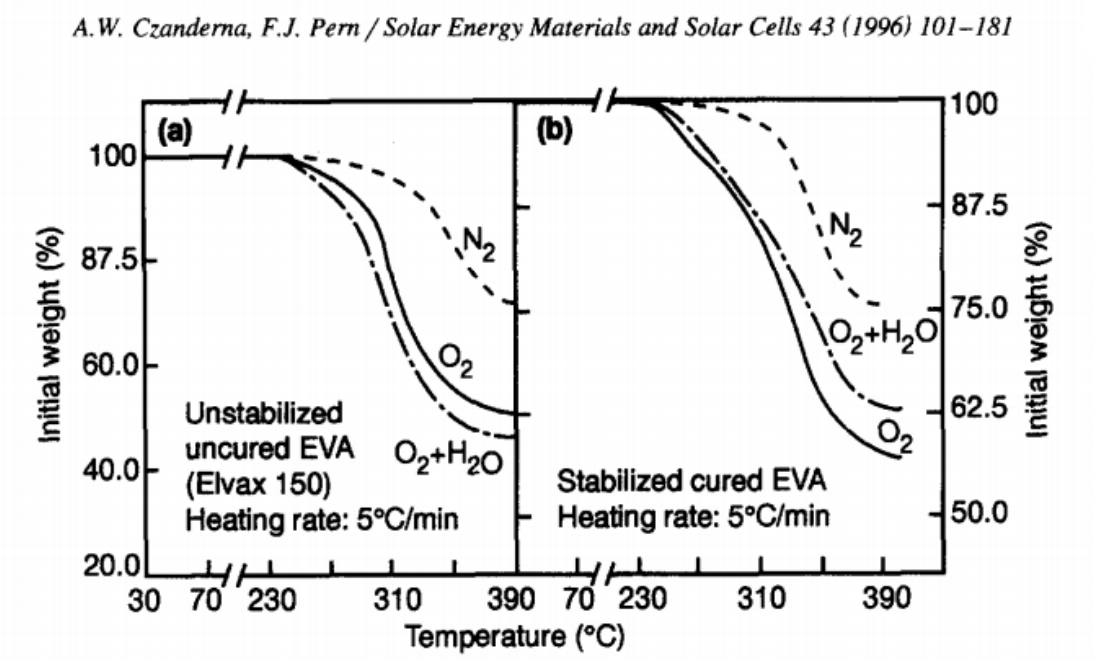

Figure 48: TGA Thermograms of Encapsulant in Various Conditions [8]

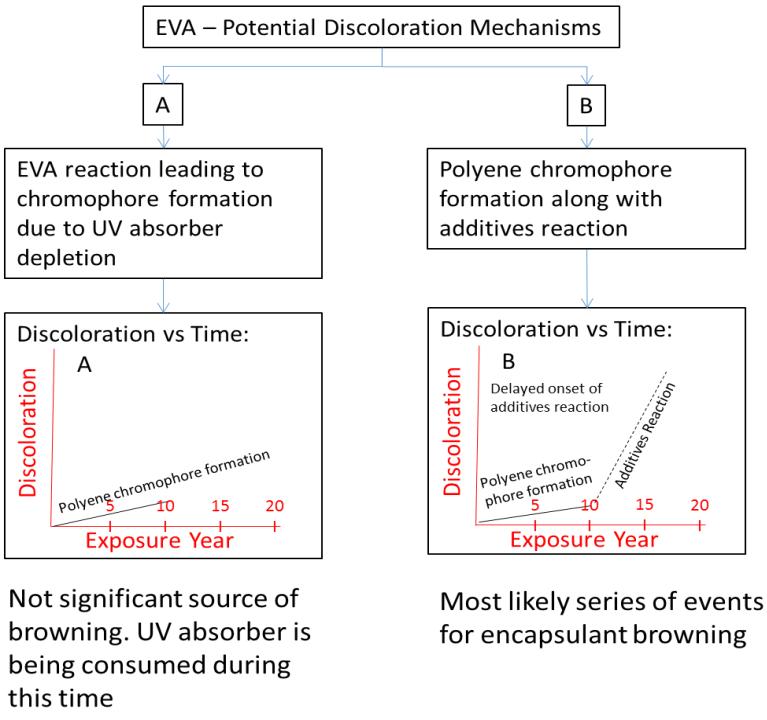

Figure 49: Degradation Overview for Encapsulant Browning

Figure 49 shows an overview of a potential mechanisms by which encapsulant used in photovoltaic modules browns. This is speculated to happen in a two-step process. The first step is the initial exposure phase (less than 10 years) where very little discoloration occurs due to polyene formation from EVA base polymer because the UV absorber is still present in the encapsulant during this time. Simultaneously happening in this step is the decomposition products of UV absorber, other additives and the Norrish II reaction of base polymer resulting in de-acetylation of the vinyl acetate copolymer. The two most important steps occurring during reaction A and B are the buildup of acetate groups resulting in an auto catalytic effect for cascading reaction, and the decomposition of the UV absorber and other additives into its degraded parts. As shown in reaction B, once the UV absorber has been thoroughly consumed, a process which has shown to take 10-15 years depending on climate conditions, the degraded products of the UV absorber in combination with other additives and acetate groups react to create chromophores at a very high rate that result in a browned EVA in a short period of time after the initial exposure phase.

CHAPTER 4

CONCLUSION

Large EVA samples from both control and aged modules were extracted by cutting the modules using a diamond wheel dremel tool attachment. The FTIR spectra seem to indicate minor polyenic production, as a result of the Norrish II reaction (Reaction A in Figure 49). The absence of UV absorber in the 28 year old California modules leads to the potential correlation that chromophore generation was a result of UV absorber degradation and additives reaction shown in reaction B of Figure 49. The role of humidity in the process of EVA browning still remains unclear. The acetic acid generated through Norrish II reaction as a byproduct may have been consumed by a corrosion reaction with metallic components of the cell as indicated by the series resistance increase. To further confirm these findings, this study needs to be extended with additional number of samples from this aged module and other aged modules which have browned EVA. Only one crystalline phase (imperfect phase) has been observed in the control samples whereas two crystalline phases (imperfect and perfect phases) have been observed in the aged samples due to higher level of cross linking in the aged samples. The broad exothermic peaks observed in the control samples around 180-210^{o}C for the cycle 2 (before recrystallization) are attributed to the presence of peroxide in EVA, could be specifically to Lubersol 101. These broad exothermic peaks do not appear in the aged samples as peroxide is already consumed or degraded over the years of exposure in the field.

REFERENCES

[1] S. V. Janakeeraman, J. Singh, J. Kuitche, J. Mallineni and G. TamizhMani "A Statistical Analysis on the Cell Parameters Responsible for Power Degradation of Fielded PV Modules in a Hot-Dry Climate," IEEE Photovoltaic Specialists Conference, June 2014.

[2] S. Shrestha, J. Mallineni, K. Yedidi, B. Knisely, S. Tatapudi, J. Kuitche, and G. TamizhMani, "Determination of Dominant Failure Modes Using FMECA on the Field Deployed c-Si Modules under Hot-Dry Desert Climate," IEEE Photovoltaic Specialists Conference, June 2014.

[3] D. L. King, M. A. Quintana, J. A. Kratochvil, D. E. Ellibee, and B. R. Hansen, "Photovoltaic Module Performance and Durability Following Long-Term Field Exposure," Progress in Photovoltaics: Research and Applications,8, 241–256, 2000.

[4] B. Knisely, J. Kuitche, G. TamizhMani, A. Korostyshevsky and H. Field, "Non-Intrusive Cell Quantum Efficiency Measurements of Accelerated Stress Tested Photovoltaic Modules," IEEE Photovoltaic Specialists Conference, June 2014.

[5] Pveducation.org, 'Anti-Reflection Coatings | PVEducation', 2015.[Online].Available: http://pveducation.org/pvcdrom/design/anti-reflection-coatings.[Accessed:13-May-2015].

[6] Pern, F. J. "Ethylene-vinyl Acetate (EVA) Encapsulants for Photovoltaic Modules Degradation and Discoloration Mechanisms and Formulation Modifications for Improved Photovisibility." N.p., n.d. Web.

[7] Chen, Shuangjun, Jun Zhang, and Jun Su. "Effect of Damp-Heat Aging on the Properties of Ethylene-Vinyl Acetate Copoylmer and Ethylene-Acrylic Acid Copolymer and Ethylene-Acrylic Copoylmer Blends." N.p., n.d. Web.

[8] Pern, F. J., and A. W. Czanderna. "Characterization of Ethylene Vinyl Acetate (EVA) Encapsulant: Effects of Thermal Processing and Weathering Degradation on Its Discoloration." N.p., n.d. Web.

[9] Wu, Dan. "Investigation of the Reliability of the Encapsulation System of Photovoltaic Modules,." N.p., n.d. Web.